[19] T. Matsui, Y. Katsuno, T. Inoue, F. Fujita, T. Joh, H. Niida, H. Murakami, M. Itoh, M. Nakanishi, Negative regulation of Chk2 expression by p53 is dependent on the CCAAT-binding transcription factor NF-Y, J. Biol. Chem. 279 (2004) 25093–250100.
[20] M. Shimada, H. Niida, D.H. Zineldeen, H. Tagami, M. Tanaka, H. Saito, M. Nakanishi, Chk1 is a histone H3 threonine 11 kinase that regulates DNA damage-induced transcriptional repression, Cell 132 (2008) 221–232.
[21] H. Niida, Y. Katsuno, B. Banerjee, M.P. Hande, M. Nakanishi, Specific role of Chk1 phosphorylations in cell survival and checkpoint activation, Mol. Cell Biol. 27 (2007) 2572–2581.
[22] O.V. Plotnikova, E.A. Golemis, E.N. Pugacheva, Cell cycle-dependent ciliogenesis and cancer, Cancer Res. 68 (2008) 2058–2061.
[23] A. Spektor, W.Y. Tsang, D. Khoo, B.D. Dynlacht, Cep97 and CP110 suppress a cilia assembly program, Cell 130 (2007) 678–690.
[24] L.M. Quarmby, M.R. Mahjoub, Caught Nek-ing: cilia and centrioles, J. Cell Sci. 118 (2005) 5161–5169.
[25] T.S. McClintock, C.E. Glasser, S.C. Bose, D.A. Bergman, Tissue expression patterns identify mouse cilia genes, Physiol. Genomics 32 (2008) 198–206.
[26] H. Nakajima, F. Toyoshima-Morimoto, E. Taniguchi, E. Nishida, Identification of a consensus motif for Plk (Polo-like kinase) phosphorylation reveals Myt1 as a Plk1 substrate, J. Biol. Chem. 278 (2003) 25277–25280.
[27] C. Visintin, B.N. Tomson, R. Rahal, J. Paulson, M. Cohen, J. Taunton, A. Amon, R. Visintin, APC/C-Cdh1-mediated degradation of the Polo kinase Cdc5 promotes the return of Cdc14 into the nucleolus, Genes Dev. 22 (2008) 79–90.

EXPERIMENTAL CELL RESEARCH 315 (2009) 809–819

available at www.sciencedirect.com

ScienceDirect

www.elsevier.com/locate/yexcr

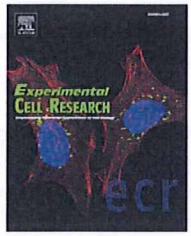

Research Article

# Disruption of the novel gene *fad104* causes rapid postnatal death and attenuation of cell proliferation, adhesion, spreading and migration

*Makoto Nishizuka*[a], *Keishi Kishimoto*[a], *Ayumi Kato*[a], *Masahito Ikawa*[b], *Masaru Okabe*[b], *Ryuichiro Sato*[c], *Hiroyuki Niida*[d], *Makoto Nakanishi*[d], *Shigehiro Osada*[a], *Masayoshi Imagawa*[a,*]

[a]*Department of Molecular Biology, Graduate School of Pharmaceutical Sciences, Nagoya City University, 3-1 Tanabe-dori, Mizuho-ku, Nagoya, Aichi 467-8603, Japan*

[b]*Genome Information Research Center, Osaka University, Yamadaoka 3-1, Suita, Osaka 565-0871, Japan*

[c]*Department of Applied Biological Chemistry, Graduate School of Agricultural and Life Sciences, The University of Tokyo, Tokyo 113-8657, Japan*

[d]*Department Cell Biology and Biochemistry, Graduate School of Medical Sciences, Nagoya City University, 1 Kawasumi, Mizuho-cho, Mizuho-ku, Nagoya, Aichi 467-8601, Japan*

ARTICLE INFORMATION

*Article Chronology:*
Received 17 July 2008
Revised version received
9 November 2008
Accepted 12 December 2008
Available online 29 December 2008

*Keywords:*
*fad104*
Adipocyte differentiation
Cell proliferation
Cell adhesion
Cell spreading
Cell migration

ABSTRACT

The molecular mechanisms at the beginning of adipogenesis remain unknown. Previously, we identified a novel gene, *fad104* (factor for adipocyte differentiation 104), transiently expressed at the early stage of adipocyte differentiation. Since the knockdown of the expression of *fad104* dramatically repressed adipogenesis, it is clear that *fad104* plays important roles in adipocyte differentiation. However, the physiological roles of *fad104* are still unknown. In this study, we generated *fad104*-deficient mice by gene targeting. Although the mice were born in the expected Mendelian ratios, all died within 1 day of birth, suggesting *fad104* to be crucial for survival after birth. Furthermore, analyses of mouse embryonic fibroblasts (MEFs) prepared from *fad104*-deficient mice provided new insights into the functions of *fad104*. Disruption of *fad104* inhibited adipocyte differentiation and cell proliferation. In addition, cell adhesion and wound healing assays using *fad104*-deficient MEFs revealed that loss of *fad104* expression caused a reduction in stress fiber formation, and notably delayed cell adhesion, spreading and migration. These results indicate that *fad104* is essential for the survival of newborns just after birth and important for cell proliferation, adhesion, spreading and migration.



* *Corresponding author.* Fax: +81 52 836 3455.
E-mail address: imagawa@phar.nagoya-cu.ac.jp (M. Imagawa).

*Abbreviations:* fad104, factor for adipocyte differentiation 104; BAT, brown adipose tissue; C/EBP, CCAAT/enhancer binding protein; Dex, dexamethasone; ER, endoplasmic reticulum; FBS, fetal bovine serum; FITC, fluorescein isothiocyanate; FNDC3a, fibronectin type III domain containing 3a; GFP, green fluorescent protein; H&E, hematoxylin and eosin; IBMX, 3-isobutyl-1-methylxantine; Ins, insulin; LC3, microtubule-associated protein light chain; MEFs, mouse embryonic fibroblasts; PBS, phosphate-buffered saline; PCR, polymerase chain reaction; PPARγ, peroxisome proliferator-activated receptor γ; RACE, rapid amplification of cDNA ends; RGS2, regulators of G protein signaling 2; SREBP-1, sterol regulatory element-binding protein 1; sys, symplastic spermatids; TCL/TC10βL, TC10 like/TC10βLong; TRITC, tetramethylrhodamine isothiocyanate; TUNEL, TdT-mediated dUTP-biotin nick end labeling; WAT, white adipose tissue

0014-4827/$ – see front matter © 2008 Elsevier Inc. All rights reserved.
doi:10.1016/j.yexcr.2008.12.013

## Introduction

Obesity is a risk factor for many diseases, such as diabetes, hypertension, hyperlipoidemia, and also arteriosclerosis [1]. Obesity is the result of an expansion of individual adipocytes and increase in the overall number of adipocytes. Therefore, to clarify the mechanism of obesity, it is necessary to elucidate the molecular mechanisms by which adipocytes differentiate. It is well established that peroxisome proliferator-activated receptor γ (PPAR γ), the CCAAT/enhancer-binding protein (C/EBP) family, and sterol regulatory element-binding protein 1 (SREBP-1) have crucial roles in the middle and the late stages of the differentiation process [2,3]. However, the events early on in adipogenesis are not fully understood.

Previously, we isolated 102 genes as inducible during the earliest stage of adipocyte differentiation with a polymerase chain reaction (PCR)-subtraction protocol [4,5]. We have identified regulators of G protein signaling 2 (RGS2), TC10-like/TC10βLong (TCL/TC10βL) and p68 RNA helicase as factors accelerating the differentiation process [6–8]. In addition, it was of interest that almost half of the isolated genes were unknown, not being present in the databases. Using the rapid amplification of cDNA ends (RACE) technique and cDNA library screening, we identified four novel genes, factor for adipocyte differentiation 24 (*fad24*), *fad123*, *fad158* and *fad104* [9–12]. Furthermore, we reported that *fad24*, *fad158* and *fad104* were positive regulators of adipocyte differentiation [9,11–13].

FAD104 is a novel protein containing 9 repeats of the fibronectin type III domain and a transmembrane domain. The expression of *fad104* was quickly and transiently elevated at the early stage of adipogenesis and was restricted to the differentiable state. Moreover, the knockdown of *fad104* by RNA interference caused inhibition of the differentiation of 3T3-L1 preadipocytes [12]. These results indicated *fad104* to have an important role in the differentiation.

The fibronectin type III domain contained in FAD104 is found in cell surface receptors and proteins regulating cell adhesion such as fibronectin and vitronectin [14,15]. Fibronectin is one of the extracellular matrix proteins and consists of three types of repeating module, called type I, type II and type III repeats. Fibronectin binds to a variety of extracellular and cell surface molecules, including integrins α5β1 and α4β1 and the HSPG coreceptor syndecan 4, and regulates cell adhesion, spreading, migration, growth and differentiation [16,17]. The Arg-Gly-Asp (RGD) tripeptide sequence in the type $III_{10}$ module of fibronectin plays an important role in the binding of the integrin receptor and activating of integrin-mediated intracellular signals [18,19]. It is of interest that *fad104* also has a RGD tripeptide sequence in the eighth fibronectin type III domain.

In addition, some previous reports indicate that the extracellular matrix proteins including fibronectin and integrins have important roles in adipogenesis [20,21]. The expression of fibronectin and integrin is downregulated during adipogenesis [20]. Furthermore, it was reported that the disruption of contacts with the extracellular matrix was required for adipocyte differentiation [21]. These reports indicate the importance of interaction between the differentiating cells and extracellular matrix, suggesting that the proteins containing the fibronectin type III domain have some crucial role in the differentiation process. However, the role of *fad104* in adipocyte conversion and various cellular functions including cell proliferation, adhesion, spreading and migration is unclear.

In this study, to gain insight into the physiological role of *fad104 in vivo*, we generated mice lacking *fad104*. Although born in the expected Mendelian ratios, the *fad104*-deficient mice all died within 1 day after birth. Interestingly although FAD104 possesses 9 repeats of the fibronectin type III domain, FAD104 localized to the endoplasmic reticulum (ER). Furthermore, analyses of mouse embryonic fibroblasts (MEFs) prepared from *fad104*-deficient mice revealed that disruption of *fad104* caused a reduction in the ability to differentiate, proliferate, adhere, spread and migrate. These results indicate that the novel gene *fad104* is essential for the survival of neonates and promotes not only adipocyte differentiation, but also cell proliferation, adhesion, spreading and migration.

## Materials and methods

### *Generation of the fad104 knockout mouse*

The targeting vector was constructed by ligating a 1.0 kb *Xho* I fragment and a 4.4 kb *Xho* I-*Sal* I fragment, which were located upstream and downstream of exon 2, respectively, to the pgk-neo cassette of pLNTK. Both the *Xho* I and *Xho* I-*Sal* I fragments were amplified by PCR using genomic DNA prepared at E14 as a template. The pgk-tk expression cassette was placed next to the short arm for negative selection against random integration. The targeting construct was linearized with the *Sal* I site and electroporated into D3 ES cells. Three positive ES cell clones, screened by Southern blot analyses, were microinjected into C57BL/6 Cr blastocysts purchased from Japan SLC (Shizuoka, Japan). The blastocysts were transferred to ICR pseudopregnant females, resulting in the birth of three lines of male chimeric mice. These male chimeric offspring were mated with C57BL/6 females and chimeras from two lines exhibited germ-line transmission. The F1 agouti offspring mice were then analyzed by Southern blotting and PCR analyses. Heterozygote male mice were backcrossed onto the C57BL/6 background for more than seven generations. All experiments were carried out according to the Guideline for the Care and Use of Laboratory Animals of Nagoya City University Medical School.

### *Genotyping*

For Southern blot analyses, genomic DNA from ES cells and tail snippets was digested with *Bam*HI-*Bgl*II, fractionated on a 1% agarose gel, and blotted onto a Hybond N+ nylon membrane (Amersham Biosciences). Homologous recombination was determined by using as a probe, 500 bp fragments located outside the targeting vector. The filter was hybridized with a probe labeled with [α-$^{32}$P]-dCTP using a random labeling kit (Takara Biomedicals). The wild-type allele produces a DNA sequence of 5. 4 kb, while the targeted DNA is 2. 0 kb long (Fig. 1A).

### *Measurements of body temperature, blood glucose level and brown adipose tissue (BAT) weight*

Newborn pups were obtained by caesarean delivery at E18.5. Just after caesarean section, a thermistor (PHYSITEMP INSTRUMENTS INC.) was introduced into the rectum of pups for body temperature measurements. BAT was isolated from the interscapular space of newborn pups, and measured its weight. Blood

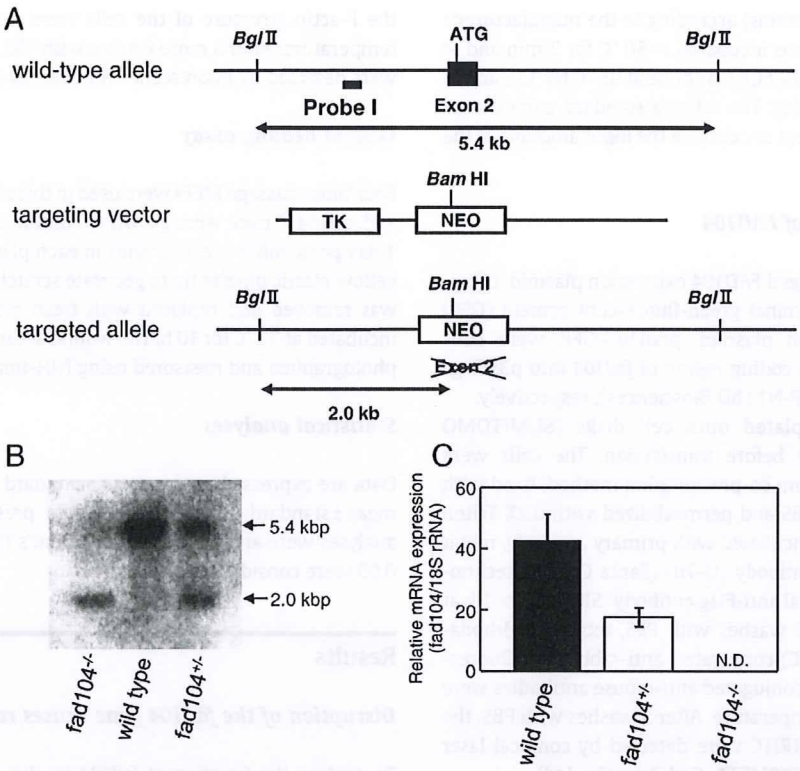


**Fig. 1 – Targeted disruption of the *fad104* gene. (A) Schematic representation of the wild-type and targeted alleles. The black box represents exon 2 of the *fad104* gene. The white boxes represent pgk-neo and pgk-tk cassettes. The probe used for Southern blot analysis is shown as Probe I. (B) Southern blot analysis of mouse genomic DNA. The expected DNA fragments for the targeted allele and the wild-type allele are 2.0 and 5. 4 kb, respectively. (C) Q-PCR analysis of mRNA from embryonic fibroblasts isolated from each of the genotypes. The expression level of *fad104* was normalized with 18S rRNA expression determined by Q-PCR. The data represent means with standard deviations ($n$=3).**

glucose level was measured by the Glucose CII-Test (Wako Pure Chemical).

### *Preparation of MEFs and adipocyte differentiation*

MEFs were isolated from decapitated embryonic day 13.5 embryos of wild type and *fad104*$^{-/-}$ mice. According to the previous reports, MEFs were used at low passage numbers (2 to 4 times) throughout the studies to avoid accumulative genetic abnormalities during passage [22,23]. Cells were cultured in α-modified Eagle's medium (α-MEM; Invitrogen) supplemented with 10% fetal bovine serum (FBS).

Induction of adipogenic differentiation was carried out according to methods described previously [24]. Briefly, MEFs (2 times passage) were seeded in culture dishes. The medium was changed to α-MEM supplemented with 0. 5 mM 3-isobutyl-1-methylxantine (IBMX), 5 μg/ml of insulin (Ins), 1 μM dexamethasone (Dex), and 10% FBS at 2 days postconfluence. This medium was renewed every other day. The amounts of triacylglycerol were measured using LIPIDOS LIQUID (Ono) according to the manufacturer's instructions.

### *Implantation and histological analyses*

MEFs (4 times passage) were grown to near confluence and trypsinized. After centrifugation, cell pellets were suspended in α-MEM containing 10% FBS and injected subcutaneously ($3\times10^7$ cells per site) with a 21-gauge needle at the back of BALB/c athymic mice (Charles River Laboratories). Three weeks after implantation, these mice were killed by cervical dislocation, and the fat pads derived from the implanted cells were excited and fixed in 10% formalin in phosphate-buffered saline (PBS). The specimens were cut into 4-μm-thick sections and stained with hematoxylin and eosin (H&E). For lipid staining with osmium tetroxide ($OsO_4$), the retrieved implants were fixed in 2.5% glutaraldehyde in PBS for 15 min and 10% formalin in PBS. To cross-link intracellular lipids, the implants were covered with a 1% $OsO_4$ solution for 2 h on ice. After excess $OsO_4$ was removed by washing with distilled water, the implants were fixed again with 10% formalin in PBS, and embedded in paraffin. The specimens were cut into 6-μm-thick sections and deparaffinized to observe $OsO_4$-stained lipids.

### *Real-time quantitative RT-PCR (Q-PCR)*

Total RNA was extracted using TRIzol (Invitrogen). For Q-PCR, cDNA was prepared using ReverTra Ace-α- (TOYOBO) following the manufacturer's recommended procedures. An ABI PRISM 7000 sequence detection system (Applied Biosystems) was used to perform Q-PCR. The pre-designed primers and probe sets of *fad104* and 18S rRNA were obtained from Applied Biosystems. The reaction mixture was prepared using a TaqMan Universal PCR

Master Mix (Applied Biosystems) according to the manufacturer's instructions. The mixture was incubated at 50 °C for 2 min and at 95 °C for 10 min, and then the PCR was done at 95 °C for 15 s and at 60 °C for 1 min for 40 cycles. The relative standard curves were generated in each experiment to calculate the input amounts of the unknown samples.

### *Subcellular localization of FAD104*

An amino terminal Flag tagged FAD104 expression plasmid, pFlag-fad104, and a carboxy terminal green-fluorescent protein (GFP) tagged FAD104 expression plasmid, pfad104-GFP, were constructed by subcloning the coding region of *fad104* into p3xFlag-CMV7.1 (SIGMA) and pEGFP-N1 (BD Biosciences), respectively.

NIH-3T3 cells were plated onto cell disks (SUMITOMO BAKELITE Co., Ltd) 1 day before transfection. The cells were transfected using the calcium co-precipitation method, fixed with 2% paraformaldehyde in PBS and permeabilized with 0.2% Triton X-100. Each cell disk was incubated with primary antibody, rabbit polyclonal anti-calnexin antibody (H-70) (Santa Cruz Biotechnology) and mouse monoclonal anti-Flag antibody (SIGMA), for 1 h at room temperature. After 5 washes with PBS, tetramethylrhodamine isothiocyanate (TRITC)-conjugated anti-rabbit and fluorescein isothiocyanate (FITC)-conjugated anti-mouse antibodies were reached for 1 h at room temperature. After 5 washes with PBS, the signals for GFP, FITC and TRITC were detected by confocal laser scanning microscopy (LSM510META, Carl Zeiss Co., Ltd).

### *Cell proliferation and cell death assay*

Two times passage MEFs were used in this study. The cells ($3\times10^4$) were seeded into 6-well tissue culture plates and trypsinized. Numbers of cells were counted at various time points during the cell growth period. For the detection of cell death, TdT-mediated dUTP-biotin nick end labeling (TUNEL) assays were performed using the In Situ Cell Death Detection kit, Fluorescein (Roche) according to the manufacturer's instructions.

### *Cell adhesion assay*

Four times passage MEFs were used in this study. The cells ($1\times10^4$) were plated onto fibronectin-coated (3 μg/ml) 24-well plates. For the coating of fibronectin, human fibronectin (SIGMA) was incubated for 1 h at room temperature. At specific time points, the unattached cells were washed away with PBS. The attached cells were fixed for 10 min in 2% paraformaldehyde in PBS at room temperature. After 3 washes with PBS, the attached cells were photographed, and counted in five random microscopic fields per plate.

### *Immunofluorescence microscopy*

Four times passage MEFs were used in this study. MEFs ($4\times10^4$) were replated on fibronectin-coated (3 μg/ml) cell disks in 24-well plates. At different time points, cell disks were fixed for 10 min in 2% paraformaldehyde in PBS and permeabilized with 0.2% Triton X-100. The cell disks were incubated with anti-vinculin monoclonal antibody (SIGMA) for 1 h at room temperature. After 3 washes with PBS, FITC-conjugated anti-mouse secondary antibody and TRITC-conjugated phalloidin (Jackson ImmunoResearch) for detection of the F-actin structure of the cells were reacted for 1 h at room temperature. After 3 more washes with PBS, FITC and TRITC signals were detected by fluorescence microscopy (BX51, OLYMPUS).

### *Wound healing assay*

Four times passage MEFs were used in this study. MEFs of wild-type and *fad104*$^{-/-}$ mice were grown to confluence in 60 mm dishes. At 1 day postconfluence, four sites in each plate were scraped with a yellow plastic pipette tip to generate scratch wounds. The medium was removed and replaced with fresh medium. The cells were incubated at 37 °C for 10 h. The wound areas at various points were photographed and measured using NIH-Image J software.

### *Statistical analyses*

Data are expressed as the mean±standard deviation (S.D.) or the mean±standard error (S.E.). All data presented with statistical analyses were analyzed using a Student's *t* test. *p* values less than 0.05 were considered to be significant.

## Results

### *Disruption of the fad104 gene causes rapid postnatal death*

To explore the function of *fad104 in vivo*, we generated *fad104*-deficient mice. We previously indicated that the mouse *fad104* was located at chromosome 3 and constituted 26 exons [12]. To disrupt the *fad104* gene, the targeting vector was designed to remove the second exon of *fad104*, which included the translational start site (Fig. 1A). The targeting vector was introduced into D3 ES cells and positive cells were selected using G418 and ganciclovir. Three of the targeted ES cell lines were injected into C57BL/6 Cr blastocysts, and chimeric male mice were obtained. Of these, two lines of mice exhibited germ-line transmission. Intercrosses of the heterozygote mice were used to establish the homozygote *fad104*-deficient mice.

First, we analyzed the genotype of mice in the heterozygote intercross at 4 weeks of age. However, *fad104*$^{-/-}$ mice were not found among 55 live-born progenies. Then, we observed the fate of the newborn mice at 1 day of birth. As shown in Table 1, ten of 47 pups obtained from crosses between heterozygote mice had already died, and three more pups died the next day. Southern blot analysis indicated that 13 newborns that died within 1 day of birth were homozygous mutants, which is almost equal to the expected Mendelian ratio (Table 1, Fig. 1B). Furthermore, Q-PCR analysis using MEFs prepared from offspring of the heterozygote intercross confirmed that *fad104*-deficient mice do not express *fad104* (Fig. 1C).

**Table 1 – Genotype of progeny of heterozygote intercrosses**

| Age | No. of mice with genotype | | |
|---|---|---|---|
| | +/+ | +/− | −/− |
| E 18.5 | 9 | 24 | 13 |
| P1 | 13 | 21 | 13[a] |
| 4-week | 19 | 36 | 0 |

[a] Ten newborns had died. Another 3 newborns died within 1 day.

To determine whether disruption of *fad104* causes lethality during embryogenesis, we next examined the genotype of newborns from the heterozygote intercross at E18.5. Just minutes after caesarean section, all pups at E18.5 were alive, and exhibited the expected Mendelian ratio (Table 1). However, all the *fad104*$^{-/-}$ offspring died within 15 min after caesarean section, whereas the wild-type and *fad104*$^{+/-}$ neonates survived. Similar results were observed for other *fad104*-deficient mice, which were obtained from independent ES clones. These results strongly suggest that the disruption of *fad104* causes rapid postnatal death.

To clarify the causes of rapid postnatal death by the disruption of *fad104*, we examined whether *fad104* is involved in the energy homeostasis just after birth (Fig. 2). We first measured the body weights and blood glucose levels of *fad104*$^{-/-}$ neonates. The body weights and blood glucose levels of *fad104*$^{-/-}$ neonates were not significantly different from those of wild-type and *fad104*$^{+/-}$ pups (Figs. 2A and B). Just after birth, the thermoregulation is very important to maintain energy homeostasis. Therefore, we next measured the body temperatures of newborn pups just after caesarean. The body temperatures did not differ among three genotypes (Fig. 2C). Furthermore, we measured weights of BAT isolated from the interscapular space of neonates. The weights of BAT of *fad104*$^{-/-}$ neonates were not also different from those of wild-type and *fad104*$^{+/-}$pups (Fig. 2D). These results may indicate that the rapid postnatal death observed in *fad104*-deficient infants is not caused by the failure of energy homeostasis.

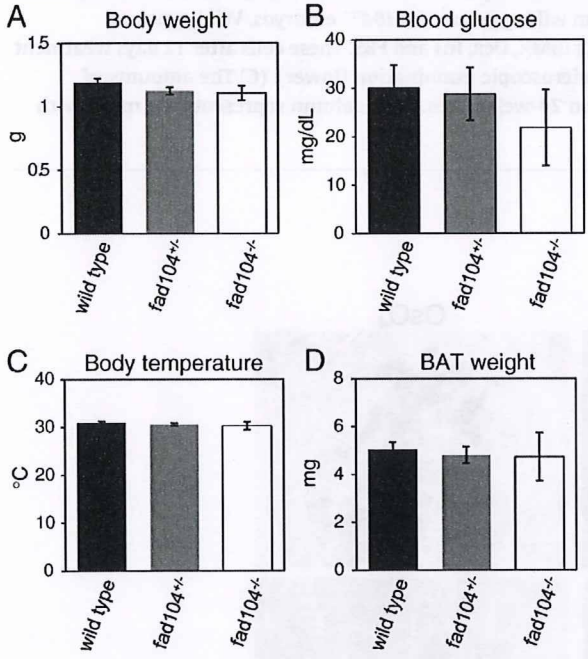


**Fig. 2 – Characterization of *fad104*-deficient mice at embryonic day 18.5. Body weights, blood glucose levels, body temperatures and BAT weights of neonates were measured just after caesarean section. (A) Body weights (wild-type, $n=17$, *fad104*$^{+/-}$, $n=36$, *fad104*$^{-/-}$, $n=9$). (B) Body temperatures (wild-type, $n=10$, *fad104*$^{+/-}$, $n=11$, *fad104*$^{-/-}$, $n=4$). (C) Blood glucose levels (wild-type, $n=12$, *fad104*$^{+/-}$, $n=14$, *fad104*$^{-/-}$, $n=5$). (D) BAT weights (wild-type, $n=10$, *fad104*$^{+/-}$, $n=11$, *fad104*$^{-/-}$, $n=4$). Each column represents the mean with standard error.**

### *Fad104-deficient MEFs exhibit reduced adipogenesis*

Since the disruption of *fad104* causes postnatal death, it is clear that *fad104* has an important role in the survival of newborn. Our previous report indicated that *fad104* promoted the differentiation of 3T3-L1 preadipocytes [12]. Therefore, using the MEFs prepared from *fad104*-deficient mice, we first examined the role of *fad104* in the conversion to adipocytes.

We investigated the expression of *fad104* during the differentiation of MEFs prepared from wild-type embryos. The level of *fad104* quickly elevated after the induction, and reached a peak at 3 h as found in 3T3-L1 cells (Fig. 3A). Next, we performed a differentiation experiment. Wild-type and *fad104*$^{-/-}$ MEFs were brought to confluence in 10% FBS. After 2 days of incubation, the medium was changed to the differentiated medium. After 12 days, the cells were stained with Oil Red O to detect oil droplets (Fig. 3B) and the amounts of triacylglycerol were determined (Fig. 3C). Under these conditions, approximately 50% of MEFs from wild-type embryos could differentiate into adipocytes. On the other hand, little accumulation of oil droplets and triacylglycerol in MEFs from *fad104*$^{-/-}$ embryos was observed.

Next, MEFs prepared from wild-type and *fad104*$^{-/-}$ embryos were implanted subcutaneously into the back of athymic mice. After 3 weeks, the implants were excited. The weights of the implants derived from *fad104*$^{-/-}$ MEFs were indistinguishable from those of wild-type MEFs (data not shown). In order to observe the histological characterization of implants, the cells accumulated oil droplets were detected by H&E and $OsO_4$ staining. The implanted wild-type MEFs developed into adipocytes and stored oil droplets. In contrast, the implanted *fad104*$^{-/-}$ MEFs failed to develop into mature adipocytes (Fig. 4). These results combined with our previous observations demonstrated that *fad104* has an important role for the differentiation of MEFs as well as of mouse 3T3-L1 cells.

### *FAD104 localized to the endoplasmic reticulum (ER)*

To determine the subcellular localization of FAD104, Flag-fad104 chimeric plasmid was transiently introduced into NIH-3T3 cells and the signals were detected by confocal scanning laser microscopy. The signals of Flag-FAD104 were observed in the cytoplasm (Fig. 5A). Because FAD104 possesses a transmembrane domain at the C-terminus, it seems that FAD104 distributes to the membrane structure in the cytoplasm. Therefore, we further conducted immunofluorescent staining using antibody against calnexin, which is a marker for the ER. The distribution of Flag-FAD104 overlapped with the staining pattern of calnexin (Fig. 5A). Since Flag-fad104 chimeric construct have Flag tag at the N-terminal site, we further constructed fad104-GFP chimeric plasmid in which GFP stays in the C terminus and introduced into NIH-3T3 cells. As shown in Fig. 5B, FAD-GFP was also distributed in the cytosol and overlapped with calnexin. These results demonstrated that the type and position of tags do not affect the distribution and FAD104 localized to the ER.

### *Cell proliferation was inhibited in fad104-deficient MEFs*

The experiments of subcellular localization of FAD104 demonstrated that FAD104 is a novel ER protein. However, it is unclear whether *fad104* is involved in cellular functions including cell proliferation, cell adhesion, cell spreading and cell migration. To elucidate the function of *fad104*, we further analyzed *fad104*-deficient MEFs.

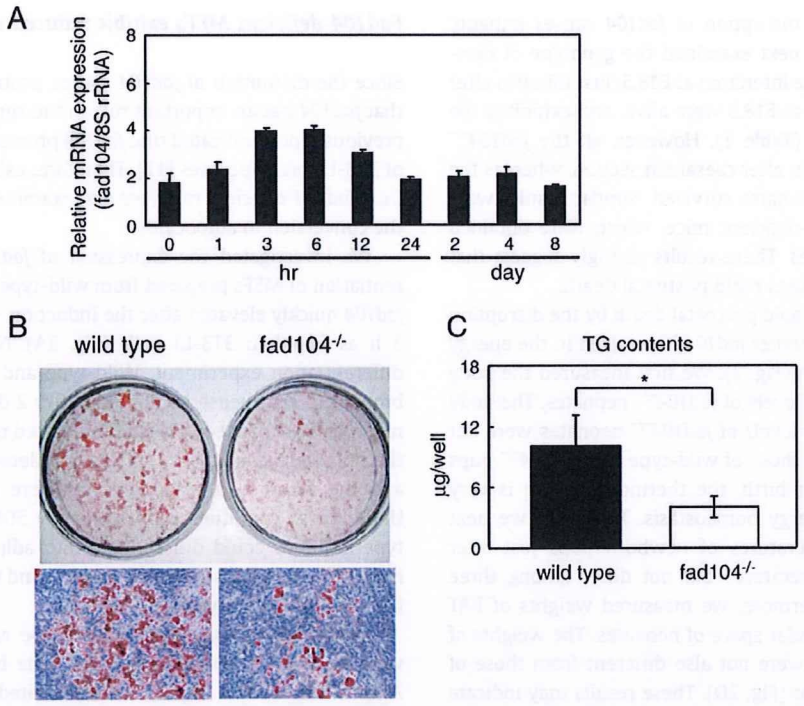


**Fig. 3 – Adipocyte differentiation of MEFs from wild-type and homozygous *fad104*-deficient embryos. (A) Q-PCR analyses of *fad104* expression in MEFs from wild-type embryos. The expression level of *fad104* was determined at various time points in the differentiation of MEFs from wild-type embryos and normalized with 18S rRNA expression determined by Q-PCR. The data represent means with standard deviations ($n=3$). (B) Differentiation of MEFs from wild-type and *fad104*$^{-/-}$ embryos. Wild-type and *fad104*$^{-/-}$ MEFs were treated with the differentiation medium containing IBMX, Dex, Ins and FBS. These cells after 12 days treatment were stained with Oil Red O. Oil Red O staining of plates (upper) and microscopic examination (lower). (C) The amounts of triacylglycerol. The measurement of triacylglycerol content was done on 24-well plates. Each column represents the mean with standard deviations ($n=3$). *$p<0.05$.**

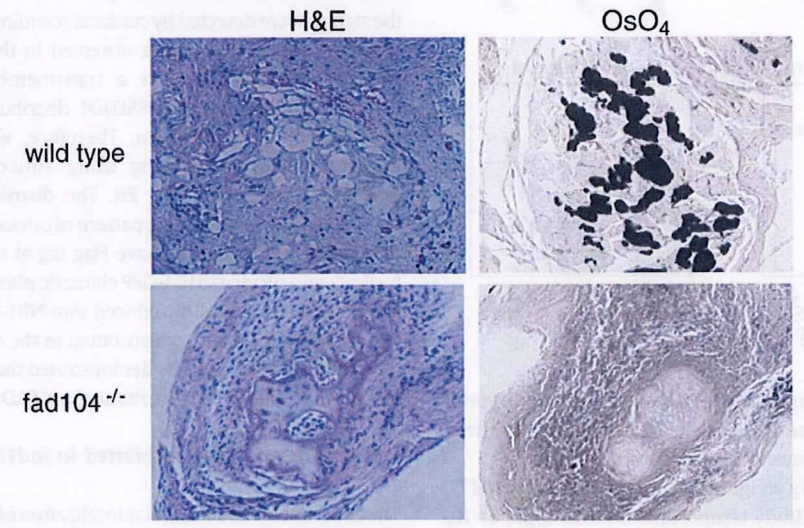


**Fig. 4 – Histological analyses of the implanted MEFs from wild-type and fad104-deficient embryo. At 3 weeks after implantation of MEFs prepared from wild-type (upper panels) and *fad104*$^{-/-}$ (lower panels) embryos, the implants were excited and stained by H&E (left panels) and $OsO_4$ (right panels).**

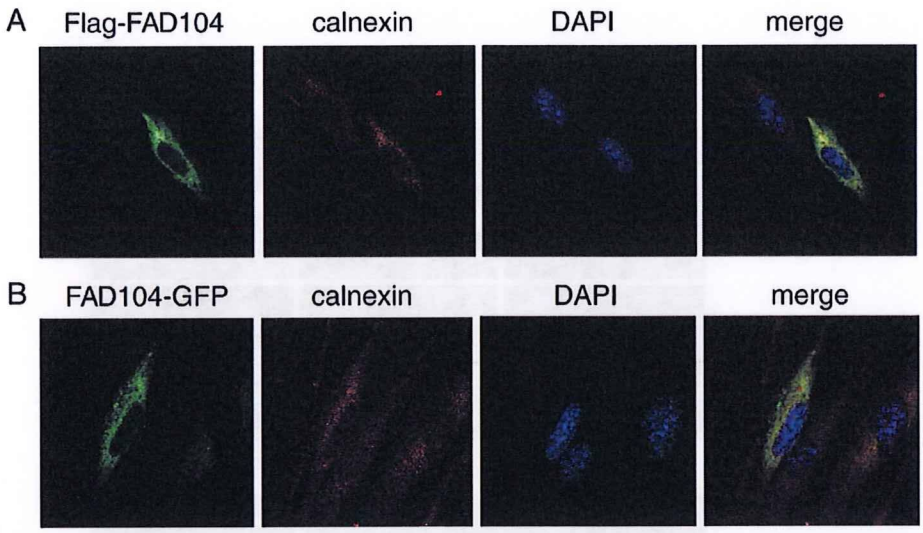


**Fig. 5 – Subcellular localization of FAD104. (A) Subcellular localization of Flag-FAD104. NIH-3T3 cells were transiently transfected with Flag-*fad104*-expression plasmid. After conducting immunofluorescent staining using anti-Flag and anti-calnexin, the signals of Flag-FAD104 (green) and calnexin (red) were detected with confocal laser scanning microscopy. (B) Subcellular localization of FAD104-GFP. NIH-3T3 cells were transiently transfected with *fad104*-GFP-expression plasmid. Transfected NIH-3T3 cells were fixed and performed the immunofluorescence analyses staining with anti calnexin. Fluorescence of FAD104-GFP (green) and calnexin (red) were detected with confocal laser scanning microscopy.**

First, we investigated the rate of cell proliferation of wild-type and *fad104*$^{-/-}$ MEFs. MEFs prepared from wild-type and *fad104*$^{-/-}$ embryos were seeded in tissue cultures, and counted at various time points. As shown in Fig. 6, the *fad104*-deficient MEFs exhibited a slightly decrease in proliferation compared with the wild-type MEFs. To exclude the possibility that the decrease of proliferating rate by the disruption of *fad104* was caused by the increase the cell death including anoixis, we performed TUNEL assay to detect cell death during proliferation in MEFs prepared from wild-type and *fad104*$^{-/-}$ embryos. At 2, 4, and 6 days after seeding, no TUNEL-positive cells were observed in wild-type and *fad104*$^{-/-}$ MEFs (data not shown). The difference of cell proliferation between wild-type and *fad104*$^{-/-}$ MEFs may not be caused by cell death. These results indicated that the disruption of *fad104* inhibits cell proliferation.

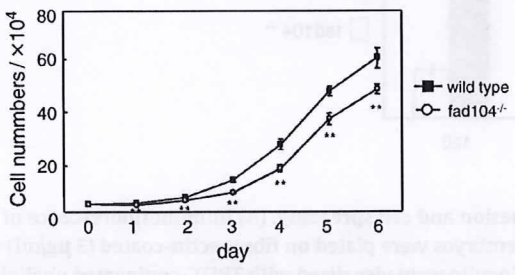


**Fig. 6 – Cell proliferation was inhibited in *fad104*-deficient MEFs. MEFs from wild-type and *fad104*$^{-/-}$ embryos were seeded in 6-well tissue culture plates at a total $3\times10^4$ cells/well. These cells were trypsinized and counted. The data represent means with standard deviations ($n$=4) $^{**}p<0.01$.**

### *Deficiency of fad104 reduced stress fiber formation and caused a delay in cell adhesion and cell spreading*

Next, to examine the effect of disruption of *fad104* on cell adhesion, cell spreading and the actin cytoskeleton's organization, we stained F-actin of wild-type and *fad104*$^{-/-}$ MEFs with TRITC-conjugated phalloidin. In addition, to detect the focal complex in wild-type and *fad104*$^{-/-}$ MEFs, the localization of vinculin was visualized using anti-vinculin antibody.

At 30 min from seeding, the wild-type MEFs already showed cell spreading and the formation of long actin stress fibers. In contrast, the *fad104*$^{-/-}$ MEFs were significantly delayed in spreading, and caused a lack of actin stress fibers and the appearance of F-actin rich membrane ruffles (Fig. 7A). At 120 min, in wild-type MEFs, the actin stress fibers were notably increased and co-localized with vinculin at the end of these fibers at focal adhesion sites. Furthermore, the morphology also changed to that of fibroblasts. In contrast, few stress fibers and morphological changes were observed in *fad104*$^{-/-}$ MEFs. In addition, vinculin in *fad104*$^{-/-}$ MEFs was not distributed to focal adhesion sites, and not co-localized with actin stress fibers (Fig. 7A). After 480 min, *fad104*$^{-/-}$ MEFs had spread more than was observed at 120 min, and developed actin stress fibers with vinculin at their ends, but were still less well spread than wild-type MEFs (Fig. 7A). These results indicated that the disruption of *fad104* reduced the numbers of stress fibers formed and cell adhesion sites, and delayed the change in cell morphology and cell spreading.

To test whether *fad104* regulates cell adhesion, we further performed a quantitative cell adhesion assay by counting the attached cells in the tissue culture. Wild-type and *fad104*$^{-/-}$ MEFs were plated onto fibronectin-coated plates. The attached cells

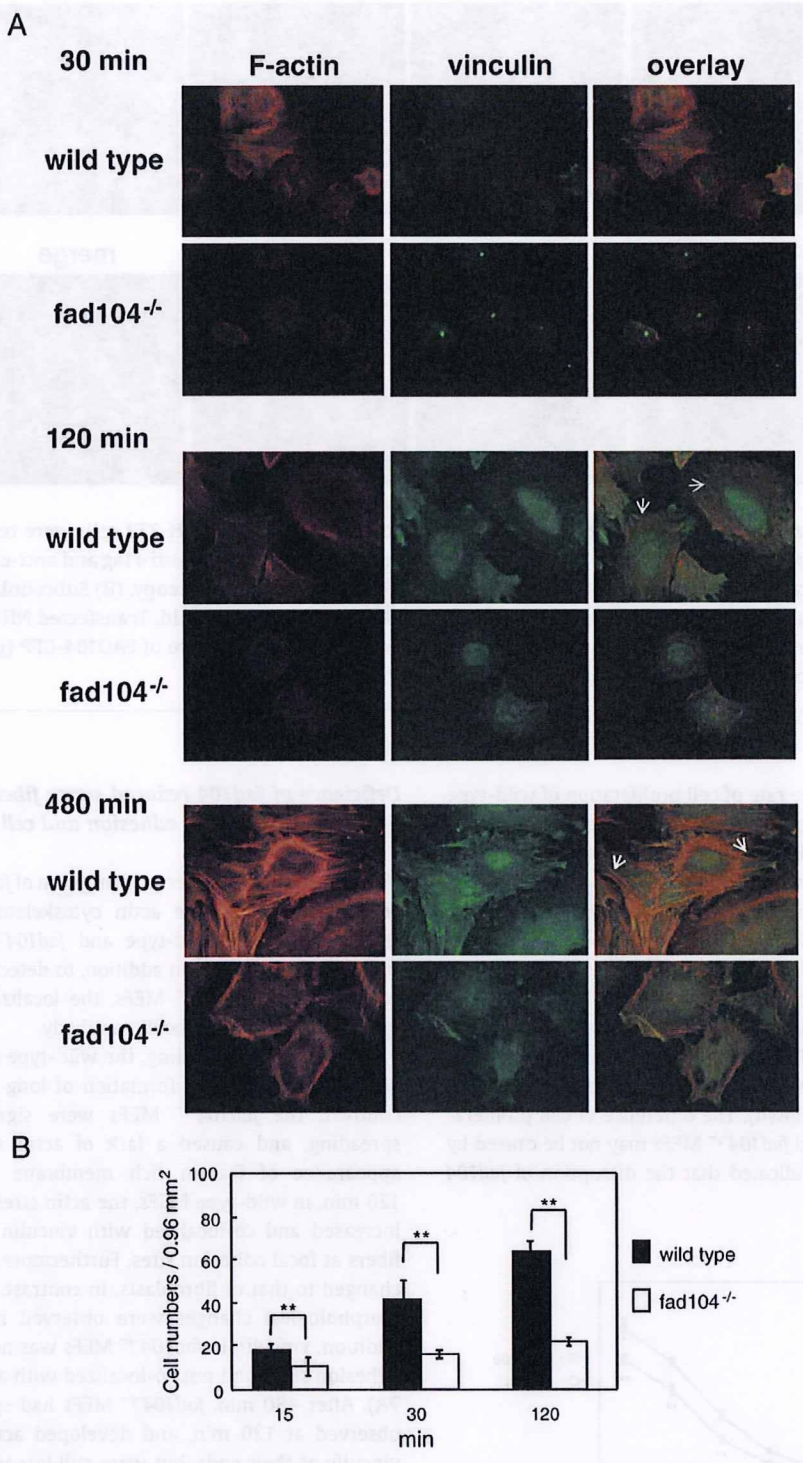


**Fig. 7 – Deletion of *fad104* causes delayed stress fiber formation, cell adhesion and cell spreading. (A) Immunofluorescence of wild-type and *fad104*$^{-/-}$ MEFs. MEFs ($4\times10^4$) from wild-type and *fad104*$^{-/-}$ embryos were plated on fibronectin-coated (3 μg/ml) cell disks in 24-well plates. At 30, 120 and 480 min from seeding, F-actin and vinculin were visualized with TRITC-conjugated phalloidin (red) and anti-vinculin antibody (green), respectively. Overlay demonstrates that the end of stress fibers co-localizes with vinculin (yellow). The arrow shows the typical end of stress fibers. A representative field at each time point is shown. (B) Cell adhesion assay of wild-type and *fad104*$^{-/-}$ MEFs. MEFs ($1\times10^4$) from wild-type and *fad104*$^{-/-}$ embryos were plated onto fibronectin-coated (3 μg/ml) 24-well plates. At each time point, the attached cells were photographed, and counted in five random microscopic fields per plate. The data represent means with standard deviations ($n=5$). $^{**}p<0.01$.**

were photographed and counted at 15, 30 and 120 min after plating. At all time points, the *fad104*$^{-/-}$ MEFs dramatically showed impaired adhesion compared with the wild-type MEFs (Fig. 7B). The results in Figs. 7A and B strongly suggest that *fad104* is a novel factor involved in cell adhesion and spreading.

### *Disruption of fad104 inhibited cell migration*

Finally, we examined the effects of disruption of *fad104* on cell migration. The ability of cells to migrate was evaluated with a wound healing assay. The confluent monolayers of wild-type and *fad104*$^{-/-}$ MEFs were wounded with a yellow tip. The damaged area was photographed and measured at the time of wounding. The wound of wild-type MEFs gradually healed and was almost closed after 10 h. On the other hand, wound closure for *fad104*$^{-/-}$ MEFs was remarkably delayed, and the wound was not completely closed within 10 h (Fig. 8A). The area of the wound that was not covered by migrating cells within 10 h was measured by NIH-Image J software (Fig. 8B). At all time points, the wound closure of *fad104*$^{-/-}$ MEFs was notably and significantly repressed compared to that of wild-type MEFs. Even after 10 h, almost half the area was still uncovered in *fad104*$^{-/-}$ MEFs. These results indicate that *fad104* is necessary for cell migration.

## Discussion

The molecular mechanism of adipocyte differentiation is very complex. Previous studies indicated that transcription factors including PPARγ, the C/EBP family and SREBP-1 regulated the differentiation process. MEFs prepared from PPARγ-deficient mice failed to differentiate into adipocytes [25]. Furthermore, the double knockout of C/EBPβ and C/EBPδ impaired the synthesis of fat in mice [24]. SREBP-1 is known to be required for production of ligands of PPARγ [26]. However, these three families of transcription factors are expressed at the middle and late stages of adipogenesis. On the other hand, it is not clear which factors regulate adipocyte differentiation at the initial stage.

Previously, we identified many genes that were expressed early on in the differentiation of 3T3-L1 cells into adipocytes [4,5]. *fad104* is a novel gene included among the isolated genes. Since knockdown of its expression inhibited the differentiation process, *fad104* has indispensable roles in the differentiation of 3T3-L1 preadipocytes. However, little was known about the functions and physiological roles of *fad104*.

In this study, to examine the actual biological functions of *fad104*, we generated mice with a homozygous null *fad104*

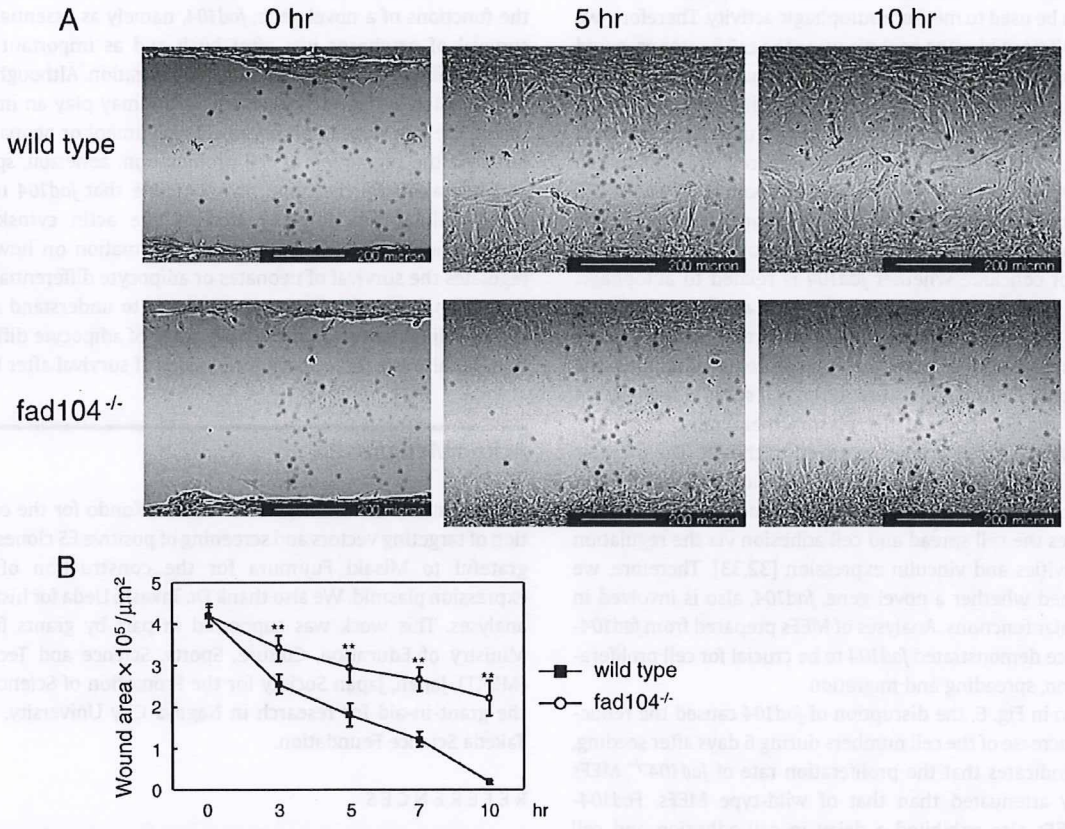


**Fig. 8 – Disruption of *fad104* inhibits cell migration in wound healing assay. (A) Wound healing assay of wild-type (top panels) and *fad104*$^{-/-}$ MEFs (bottom panels). MEFs were plated and grown to confluence. At 1 day postconfluence, a wound was introduced into the monolayer, and the migration of cells was monitored using photographs taken at time points from 0 to 10 h. The 0, 5 and 10 h time points are shown for each cell line. (B) Quantification of the wound healing assay shown in panel A. For each cell line, the wound area was quantified by using NIH-Image J software. The data represent means with standard deviations ($n$=4). **$p$<0.01.**

mutation. Interestingly, the *fad104*-deficient mice died within 1 day of birth. All of the *fad104*-deficient pups at E18.5 were breathing and moving just after caesarean section, suggesting that the disruption of *fad104* caused rapid postnatal death. It is well known that the maintenance of blood glucose levels and the thermoregulation have pivotal roles for survival of newborn pups just after birth [27,28]. However, as shown Fig. 2, *fad104*-deficient neonates did not exhibit the abnormalities about blood glucose level, body temperature, and BAT weight. In our previous reports, *fad104* was found to be highly expressed in white adipose tissue (WAT). On the other hand, *fad104* was also modestly expressed in heart, kidney and lung [12]. Since little WAT is found in newborns, it is possible that the postnatal lethality observed in *fad104*-deficient mice is caused by a functional disorder of *fad104* in organs including the heart, kidney and lung. In order to elucidate the cause of the rapid death after birth of *fad104*-deficient mice, a pathological analysis of these organs is now ongoing.

Kuma et al. indicated that mice deficient for *Atg5*, which is essential for autophagosome formation, die within 1 day at birth, suggesting that autophagic degradation of proteins is important for survival during neonatal starvation [29]. We attempted to examine whether *fad104* is involved in the regulation of autophagic activity. During autophagy, microtubule-associated protein light chain (LC3) is processed from the cytosolic form, LC3-I, to the membrane-bound form, LC3-II. Since the amount of LC3-II correlates with the number of autophagosomes, immnoblotting of endogenous LC3 can be used to measure autophagic activity. Therefore, we performed Western blotting analysis using the cell lysates prepared from wild-type and *fad104*$^{-/-}$ MEFs under nutrition starvation. Commercially available anti-LC3 antibody, which was employed the detection of endogenous LC3 in MEFs was used [30]. However, we could detect neither LC3-I nor LC3-II in the cell lysates prepared from wild-type and *fad104*$^{-/-}$ MEFs, whereas both LC3-I and LC3-II proteins were detected in the cell lysate prepared from HeLa cells under starvation condition as described previously [31]. Although we could not conclude whether *fad104* is related to autophagic activity in this study, it is necessary to elucidate the relationship between *fad104* and autophagic activity by further analyses.

Although it is well known that the proteins containing the fibronectin type III domain localize to the cell surface, the FAD104 localized to the ER, but not the plasma membrane. Therefore, FAD104 may be a novel protein localized to the ER. The proteins found in the ER have an important role of various cellular functions. For example, calreticulin, a $Ca^{2+}$-binding protein of the ER, influences the cell spread and cell adhesion via the regulation of c-Src activities and vinculin expression [32,33]. Therefore, we next examined whether a novel gene, *fad104*, also is involved in various cellular functions. Analyses of MEFs prepared from *fad104*-deficient mice demonstrated *fad104* to be crucial for cell proliferation, adhesion, spreading and migration.

As shown in Fig. 6, the disruption of *fad104* caused the reduction of the increase of the cell numbers during 6 days after seeding. This result indicates that the proliferation rate of *fad104*$^{-/-}$ MEFs was slightly attenuated than that of wild-type MEFs. *Fad104*-deficient MEFs also exhibited a delay in cell adhesion and cell spreading (Fig. 7). It is necessary to explore the mechanism which *fad104* regulates the cell proliferation.

Cell migration, cell spreading and adhesive properties are regulated by continuous remodeling of the actin cytoskeleton. For example, in cell migration, the actin structures are divided into three steps; the lamelipodial actin network at the leading edge of the cell, filopodial bundles beneath the plasma membrane, and contractile actin stress fibers in the cytoplasm [34]. At the early stage of adipocyte differentiation, the change to the actin organization is very important. Kawaguchi et al. indicated that ADAM12, a disintegrin and metalloprotease, altered the organization of the actin cytoskeleton and extracellular matrix by impairing the function of β1 integrin, and induced differentiation into mature adipocytes [35]. A deficiency of *fad104* dramatically reduces the formation of stress fibers, strongly suggesting that *fad104* also functions as a key regulator of the actin cytoskeleton's organization, and may promote adipogenesis in the early stages of the differentiation process.

Recently, Obholz et al. reported that a fibronectin type III domain containing 3a (FNDC3A) is necessary for adhesion between spermatids and Sertoli cells, and the mutation of *fndc3a* is the cause of male sterility in symplastic spermatids (sys) mice [36]. FNDC3a is closely related to FAD104, since FNDC3a also contains 9 repeats of the fibronectin type III domain and transmembrane domain. It is of interest that FNDC3a is also necessary for mediating adhesion during spermatogenesis. However, FNDC3a does not have a RGD tripeptide sequence in any fibronectin type III domain repeat sequence. In addition, the disruption of FNDC3a does not cause postnatal death. Thus, although FAD104 and FNDC3a are very similar, these two proteins might have distinct and different roles in cellular functions and developmental processes.

In summary, the present study provided some new insights into the functions of a novel gene, *fad104*, namely as essential for the survival of newborns just after birth and as important for cell proliferation, adhesion, spreading and migration. Although further investigation is definitely needed, *fad104* may play an important role in the late stage of embryonic development or neonates after birth via the regulation of cell proliferation, adhesion, spreading and migration. Furthermore, it is possible that *fad104* regulates these cellular functions by altering the actin cytoskeleton's organization. Although we have no information on how *fad104* regulates the survival of neonates or adipocyte differentiation yet, further analyses of *fad104* would help us to understand not only the signaling pathways at the early stage of adipocyte differentiation but also the molecular mechanisms of survival after birth.

## Acknowledgments

We thank Dr. Kei Tominaga and Chiharu Kondo for the construction of targeting vectors and screening of positive ES clones. We are grateful to Misaki Fujimura for the construction of fad104 expression plasmid. We also thank Dr. Takashi Ueda for histological analyses. This work was supported in part by grants from the Ministry of Education, Culture, Sports, Science and Technology (MEXT), Japan, Japan Society for the Promotion of Science (JSPS), the grant-in-aid for research in Nagoya City University, and the Takeda Science Foundation.

REFERENCES

[1] P.G. Kopelman, Obesity as a medical problem, Nature 404 (2000) 635–643.
[2] R.P. Brun, J.B. Kim, E. Hu, S. Altiok, B.M. Spiegelman, Adipocyte differentiation: a transcriptional regulatory cascade, Curr. Opin. Cell Biol. 8 (1996) 826–832.

[3] E.D. Rosen, C.J. Walkey, P. Puigserver, B.M. Spiegelman, Transcriptional regulation of adipogenesis, Genes Dev. 14 (2000) 1293–1307.
[4] M. Imagawa, T. Tsuchiya, T. Nishihara, Identification of inducible genes at the early stage of adipocyte differentiation of 3T3-L1 cells, Biochem. Biophys. Res. Commun. 254 (1999) 299–305.
[5] M. Nishizuka, T. Tsuchiya, T. Nishihara, M. Imagawa, Induction of Bach1 and ARA70 gene expression at an early stage of adipocyte differentiation of mouse 3T3-L1 cells, Biochem. J. 361 (2002) 629–633.
[6] M. Nishizuka, K. Honda, T. Tsuchiya, T. Nishihara, M. Imagawa, RGS2 promotes adipocyte differentiation in the presence of ligand for peroxisome proliferator-activated receptor gamma, J. Biol. Chem. 276 (2001) 29625–29627.
[7] M. Nishizuka, E. Arimoto, T. Tsuchiya, T. Nishihara, M. Imagawa, Crucial role of TCL/TC10beta L, a subfamily of Rho GTPase, in adipocyte differentiation, J. Biol. Chem. 278 (2003) 15279–15284.
[8] A. Kitamura, M. Nishizuka, K. Tominaga, T. Tsuchiya, T. Nishihara, M. Imagawa, Expression of p68 RNA helicase is closely related to the early stage of adipocyte differentiation of mouse 3T3-L1 cells, Biochem. Biophys. Res. Commun. 287 (2001) 435–439.
[9] K. Tominaga, Y. Johmura, M. Nishizuka, M. Imagawa, Fad24, a mammalian homolog of Noc3p, is a positive regulator in adipocyte differentiation, J. Cell. Sci. 117 (2004) 6217–6226.
[10] K. Tominaga, T. Kagata, Y. Johmura, T. Hishida, M. Nishizuka, M. Imagawa, SLC39A14, a LZT protein, is induced in adipogenesis and transports zinc, FEBS J. 272 (2005) 1590–1599.
[11] K. Tominaga, C. Kondo, T. Kagata, T. Hishida, M. Nishizuka, M. Imagawa, The novel gene fad158, having a transmembrane domain and leucine-rich repeat, stimulates adipocyte differentiation, J. Biol. Chem. 279 (2004) 34840–34848.
[12] K. Tominaga, C. Kondo, Y. Johmura, M. Nishizuka, M. Imagawa, The novel gene fad104, containing a fibronectin type III domain, has a significant role in adipogenesis, FEBS Lett. 577 (2004) 49–54.
[13] Y. Johmura, S. Osada, M. Nishizuka, M. Imagawa, FAD24 acts in concert with histone acetyltransferase HBO1 to promote adipogenesis by controlling DNA replication, J. Biol. Chem. 283 (2008) 2265–2274.
[14] D. Craig, M. Gao, K. Schulten, V. Vogel, Structural insights into how the MIDAS ion stabilizes integrin binding to an RGD peptide under force, Structure 12 (2004) 21–30.
[15] R. Pankov, K.M. Yamada, Fibronectin at a glance, J. Cell. Sci. 115 (2002) 3861–3863.
[16] S.K. Sastry, K. Burridge, Focal adhesions: a nexus for intracellular signaling and cytoskeletal dynamics, Exp. Cell Res. 262 (2000) 25–36.
[17] B.H. Geiger, A. Bershadsky, R. Pankov, K.M. Yamada, Transmembrane crosstalk between the extracellular matrix–cytoskeleton crosstalk, Nat. Rev. Mol. Cell Biol. 2 (2002) 793–805.
[18] R.D. Bowditch, M. Hariharan, E.F. Tominna, J.W. Smith, K.M. Yamada, E.D. Getzoff, M.H. Ginsberg, Identification of a novel integrin binding site in fibronectin. Differential utilization by beta 3 integrins, J. Biol. Chem. 269 (1994) 10856–10863.
[19] T. Nagai, N. Yamakawa, S. Aota, S.S. Yamada, S.K. Akiyama, K. Olden, K.M. Yamada, Monoclonal antibody characterization of two distant sites required for function of the central cell-binding domain of fibronectin in cell adhesion, cell migration, and matrix assembly, J. Cell Biol. 114 (1991) 1295–1305.
[20] B.M. Spiegelman, S.D. Farmer, Decreases in tubulin and actin gene expression prior to morphological differentiation of 3T3 adipocytes, Cell 29 (1982) 53–60.
[21] B.M. Spiegelman, C.A. Ginty, Fibronectin modulation of cell shape and lipogenic gene expression in 3T3-adipocytes, Cell 35 (1983) 657–666.
[22] L. Yang, L. Wang, Y. Zheng, Gene targeting of Cdc42 and Cdc42GAP affirms the critical involvement of Cdc42 in filopodia induction, directed migration, and proliferation in primary mouse embryonic fibroblasts, Mol. Biol. Cell 17 (2006) 4675–4685.
[23] F. Chen, Y. Lu, V. Castranova, Z. Li, M. Karin, Loss of IKKβ promotes migration and proliferation of mouse embryo fibroblast cells, J. Biol. Chem. 281 (2006) 37142–37149.
[24] T. Tanaka, N. Yoshida, T. Kishimoto, S. Akira, Defective adipocyte differentiation in mice lacking the C/EBPbeta and/or C/EBPdelta gene, EMBO J. 16 (1997) 7432–7443.
[25] N. Kubota, Y. Terauchi, H. Miki, H. Tamemoto, T. Yamauchi, K. Komeda, S. Satoh, R. Nakano, C. Ishii, T. Sugiyama, K. Eto, Y. Tsubamoto, A. Okuno, K. Murakami, H. Sekihara, G. Hasegawa, M. Naito, Y. Toyoshima, S. Tanaka, K. Shiota, T. Kitamura, T. Fujita, O. Ezaki, S. Aizawa, R. Nagai, K. Tobe, S. Kimura, T. Kadowaki, PPAR gamma mediates high-fat diet-induced adipocyte hypertrophy and insulin resistance, Mol. Cell 4 (1999) 597–609.
[26] J.B. Kim, B.M. Spiegelman, ADD1/SREBP1 promotes adipocyte differentiation and gene expression linked to fatty acid metabolism, Genes Dev. 10 (1996) 1096–1107.
[27] B. Cannon, J. Nedergaard, Brown adipose tissue: function and physiological significance, Physiol. Rev. 84 (2004) 277–359.
[28] M.E. Symonds, M.A. Lomax, Material and environmental influences on thermoregulation in the neonate, Proc. Nutr. Soc. 51 (1992) 165–172.
[29] A. Kuma, M. Hatano, M. Matsui, A. Yamamoto, H. Nakaya, T. Yoshimori, Y. Ohsumi, T. Tokuhisa, N. Mizushima, The role of autophagy during the early neonatal starvation period, Nature 432 (2004) 1032–1035.
[30] C.P. Cheng, M.C. Yang, H.S. Liu, Y.S. Lin, H.Y. Lei, Concanavalin A induces autophagy in hepatoma cells and has a therapeutic effect in a murine in situ hepatoma model, Hepatology 45 (2007) 286–296.
[31] Y. Kabeya, N. Mizushima, T. Ueno, A. Yamamoto, T. Kirisako, T. Noda, E. Kominami, Y. Ohsumi, T. Yoshimori, LC3, a mammalian homologue of yeast Apg8p, is localized in autophagosome membranes after processing, EMBO J. 19 (2000) 5720–5728.
[32] S. Papp, M.P. Fadel, H. Kim, C.A. McCulloch, M. Opas, Calreticulin affects fibronectin-based cell-substratum adhesion via the regulation of c-Src activity, J. Biol. Chem. 282 (2007) 16585–16598.
[33] M. Opas, M.S. Pawlikowski, G.K. Jass, N. Mesaeli, M. Michalak, Calreticulin modulates cell adhesiveness via regulation of vinculin expression, J. Cell Biol. 135 (1996) 1913–1923.
[34] P. Hatulainen, P. Lappalainen, Stress fibers are generated by two distinct actin assembly mechanisms in motile cells, J. Cell Biol. 173 (2006) 383–394.
[35] N. Kawaguchi, C. Sundberg, M. Kveiborg, B. Moghadaszadeh, M. Asmar, N. Dietrich, C.K. Thodeti, F.C. Nielson, P. Moller, A.M. Mercurio, R. Albrechtsen, U.M. Wewer, ADAM12 induces actin cytoskeleton and extracellular matrix reorganization during early adipocyte differentiation by regulating beta1 integrin function, J. Cell. Sci. 116 (2003) 3893–3904.
[36] K.L. Obholz, A. Akopyan, K.G. Waymire, G.R. MacGregor, FNDC3A is required for adhesion between spermatids and Sertoli cells, Dev. Biol. 298 (2006) 498–513.

Biochemical and Biophysical Research Communications 388 (2009) 529–532

Contents lists available at ScienceDirect

Biochemical and Biophysical Research Communications

journal homepage: www.elsevier.com/locate/ybbrc

# Casein kinase II is required for the spindle assembly checkpoint by regulating Mad2p in fission yeast

Midori Shimada [a], Ayumu Yamamoto [b], Yuko Murakami-Tonami [a,1], Makoto Nakanishi [a], Takashi Yoshida [a], Hirofumi Aiba [c], Hiroshi Murakami [a,*]

[a] Department of Biochemistry and Cell Biology, Graduate School of Medicine, Nagoya City University, 1 Kawasumi, Mizuho-cho, Mizuho-ku, Nagoya 467-8601, Japan
[b] Department of Chemistry, Shizuoka University, 836 Ohya, Suruga-ku, Sizuoka 422-8529, Japan
[c] Laboratory of Molecular Microbiology, School of Agriculture, Nagoya University, Chikusa-ku, Nagoya 464-8601, Japan

ARTICLE INFO

*Article history:*
Received 4 August 2009
Available online 8 August 2009

*Keywords:*
Cell cycle
*Schizosaccharomyces pombe*
Mitosis

ABSTRACT

The spindle checkpoint is a surveillance mechanism that ensures the fidelity of chromosome segregation in mitosis. Here we show that fission yeast casein kinase II (CK2) is required for this checkpoint function. In the CK2 mutants mitosis occurs in the presence of a spindle defect, and the spindle checkpoint protein Mad2p fails to localize to unattached kinetochores. The CK2 mutants are sensitive to the microtubule depolymerising drug thiabendazole, which is counteracted by ectopic expression of *mad2*$^+$. The level of Mad2p is low in the CK2 mutants. These results suggest that CK2 has a role in the spindle checkpoint by regulating Mad2p.



## Introduction

Cell cycle checkpoints monitor cell cycle progression to ensure the integrity of the genome and the fidelity of sister chromatid separation [1–3]. In most eukaryotes, the spindle assembly checkpoint (SAC) is a surveillance mechanism that delays anaphase onset until all chromosomes are correctly attached in a bipolar fashion to the mitotic spindle [4]. This checkpoint prevents chromosome mis-segregation during mitosis. The main spindle checkpoint proteins, which include Mad1, Mad2, BubR1 (Mad3 in yeast), Bub1, Bub3, and Mps1, have been identified [4] and are conserved in all eukaryotes. Additionally, there are several structural components of the kinetochore and centromere whose functions are required to sustain the checkpoint, such as the Ndc80, Mcm21, Mtw1 complexes and centromere proteins A (CENP-A), C, E, F, I [5,6]. Several other checkpoint components, such as Zw10 and Rod, have been identified in higher eukaryotes but have no yeast orthologues [7]. Recently, it was reported that the conserved human PRP4 protein kinase, which is implicated in the regulation of mRNA splicing, is required for the SAC [8].

The SAC acts by inhibiting the anaphase promoting complex or cyclosome (APC/C), a multi-subunit ubiquitin ligase required to promote degradation of both the anaphase inhibitor securin and B-type cyclins [9,10]. Degradation of securin and cyclin triggers chromosome segregation at the metaphase-anaphase transition and exit from mitosis, respectively. APC/C inhibition during checkpoint activation is mediated by a direct interaction of Mad2p with the Slp1p/Cdc20 protein. In fission yeast, as well as in other organisms, Mad2p localizes to unattached kinetochores upon activation of the SAC [11].

We have been studying the relationships among cell cycle controls induced by DNA replication inhibition, DNA damage, spindle assembly defects and RNA splicing defects [12,13]. We have isolated a casein kinase II (CK2) mutant (*orb5-3c13*) that is defective in arrest induced by RNA splicing defects but not by the replication and DNA damage checkpoints [12]. CK2 is a highly conserved serine-threonine kinase that is typically found in tetrameric complexes consisting of two catalytic (α and/or α′) subunits and two β regulatory subunits [14]. In fission yeast, Orb5p is a catalytic subunit of CK2, whereas Ckb1p is a regulatory subunit [15]. Here, we investigate the function of CK2 in the SAC.

## Materials and methods

*Yeast strains, media, and genetic methods.* Complete medium (YES) and minimal medium (EMM) were prepared and standard methods were used as described [16]. Procedures for gene disruption and COOH-terminal tagging of proteins with the HA, Myc, or GFP epitope were previously described [17]. Transformation of *Schizosaccharomyces pombe* was performed by the lithium method [18]. For microscopic analysis, cells were fixed with 70% ethanol and stained with 4′,6-diamidino-2-phenylindole (DAPI) as described [19]. The *S. pombe* strains used in this study included HM4 [*h*$^-$ *leu1-32*], HM817 [*h*$^+$ *leu1-32 nda3-311*], HM1338

* Corresponding author. Fax: +81 52 842 3955.
*E-mail address:* hmura@med.nagoya-cu.ac.jp (H. Murakami).
[1] Present address: Department of Biochemistry, Nagoya University Graduate School of Medicine, 65 Tsurumai-cho, Showa-ku, Nagoya 466-8550, Japan.

0006-291X/$ - see front matter © 2009 Elsevier Inc. All rights reserved.
doi:10.1016/j.bbrc.2009.08.030

[*h*⁺ *leu1-32 ura4-D18 mad2::ura4*⁺], HM3434 [*h*⁻ *leu1-32 orb5-3c13*], HM3584 [*h*⁻ *leu1-32 ckb1::kan*], HM3625 [*h*⁻ *leu1-32 ura4-D18 ckb1-3HA-kan*], HM4846 [*h*⁻ *leu1-32 ura4-D18 nda3-311 mad2::ura4*⁺], HM4956 [*h*⁻ *leu1-32 nda3-311 orb5-3c13*], HM4957 [*h*⁻ *leu1-32 nda3-311 ckb1::kan*], HM5172 [*h*⁻ *leu1-32 ckb1::kan mad2-GFP-kan*], HM5177 [*h*⁺ *leu1-32 ura4-D18 ckb1::kan mad2::ura4*⁺], HM5210 [*h*⁻ *leu1-32 nda3-311 ckb1-3HA-kan*], HM5213 [*h*⁻ *leu1-32 nda3-311 ckb1-GFP-kan*], HM5265 [*h*⁻ *leu1-32 orb5-3c13 mad2-GFP-kan*], HM5170 [*h*⁻ *leu1-32 nda3-311 mad2-GFP-kan*], and HM5741 [*h*⁻ *leu1-32 ura4-D18 nda3-311 ckb1::kan mad2-GFP-kan*], and HM5867 [*h*⁻ *leu1-32 ura4-D18 nda3-311 orb5-GFP-kan*].

*Protein extraction and western blotting.* Protein extracts were prepared and western blotting was performed as described [19]. Mouse monoclonal antibodies to HA (1:1000 dilution, Roche), GFP (1:1000 dilution, Roche) and α-tubulin (1:50,000 dilution, Sigma) were used. Immune complexes were detected with HRP-conjugated anti-mouse or anti-rabbit secondary antibodies (both at 1:1000 dilution, Amersham) and ECL reagents (Amersham).

*Preparation of synchronous cultures.* $G_2$ cells were synchronized using 7–30% lactose gradients as described [12]. The percentage of cells that had passed mitosis was determined microscopically by ascertaining the number of cells that had begun or finished septation; this number was then divided by the total number of cells, and the quotient was multiplied by 100.

## Results and discussion

We reasoned that if casein kinase II (CK2) functions as a spindle checkpoint protein in fission yeast, cells deficient in CK2 may be hypersensitive to microtubule-destabilizing drugs such as thiabendazole (TBZ), because of their inability to arrest cell cycle progression in the presence of a defective spindle. The *orb5* mutant (*orb5-3c13*) was viable, but its growth rate was reduced at high temperature (Fig. 1A) [12]. This strain was hypersensitive to TBZ (Fig. 1A). Cells lacking *ckb1* are viable but have a cold-sensitive phenotype [15], and they were also hypersensitive to TBZ.

To determine whether cells harboring defective CK2 proteins are also sensitive to other spindle defects, we tested for synthetic lethality among CK2 and *nda3* mutants, which are defective in the β-tubulin gene (Fig. 1B). At a restrictive temperature *nda3-311* mutants arrest at prometaphase and lack a mitotic spindle due to a cold-sensitive mutation [20]. Both *ckb1* and *nda3* single mutants maintained high viability at 32 °C. In contrast, the *nda3 ckb1* double mutant rapidly lost viability at all temperatures tested. However, the viability of the *nda3 orb5* double mutant was similar to that of the *nda3* mutant. This may be because the *orb5* mutant is temperature-sensitive. These findings suggest that CK2 mutants lose viability when spindles are defective.

Given that we identified CK2 as having a potential role in the SAC in *nda3* cells, we further investigated the phenotype of CK2 mutants. We synchronized mutants in early $G_2$ phase by lactose gradient centrifugation, shifted the temperature to 18 °C at time 0 and monitored mitotic progression (Fig. 1C). Whereas *wt* cells underwent nuclear division ~120 min after the temperature shift, *nda3 mad2* cells did so later. In contrast to *nda3* cells, *nda3 ckb1* cells underwent nuclear division, although progression through mitosis was somewhat delayed compared with that in *mad2 nda3* cells, probably due to the slow growth of *nda3 ckb1* cells at low temperature. *nda3 orb5* cells also underwent nuclear division, although their progression through mitosis was severely delayed (data not shown). These results suggest that CK2 is required for the SAC.

Mad2p localizes to unattached kinetochores [11] and this localization is believed to be required for activation of the checkpoint.

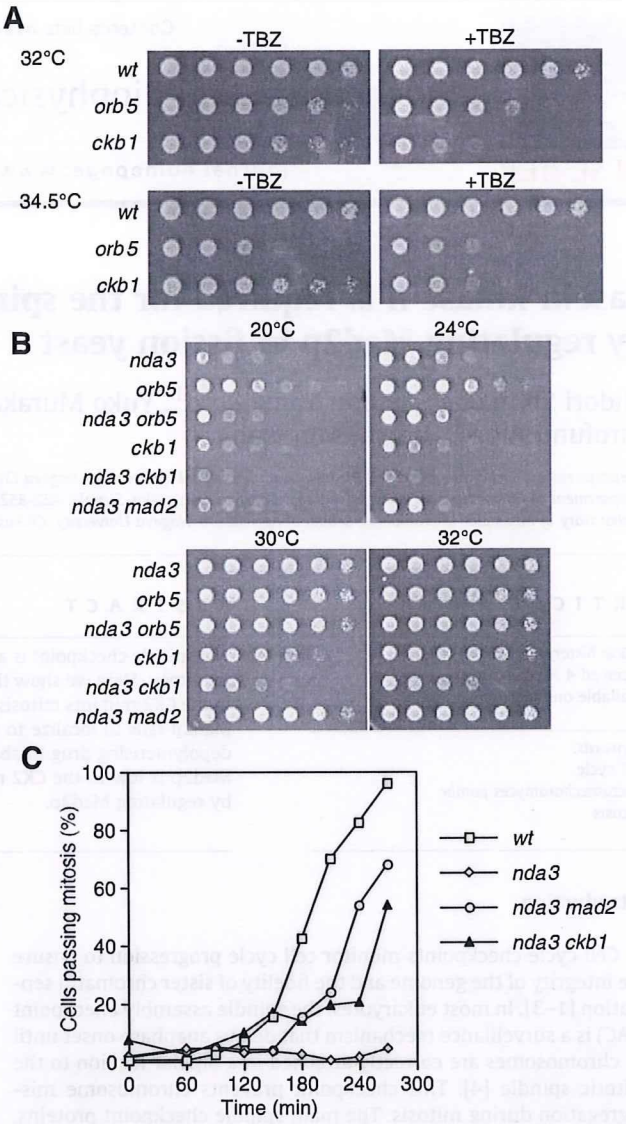


**Fig. 1.** CK2 is required for the spindle assembly checkpoint. (A, B) Cells of the indicated genotypes (*wt*, HM4; *orb5*, HM3434; *ckb1*, HM3584; *nda3*, HM817; *nda3 orb5*, HM4956; *nda3 ckb1*, HM4957; *nda3 mad2*; and HM4846) were grown exponentially and spotted onto YES plates with or without 0.015 mg/ml TBZ and incubated at the indicated temperatures for 2 days. (C) Cells of the indicated genotypes in (A), (B) were grown to mid-log phase in YES medium at 32 °C, and those in early G2 phase were collected by lactose gradient centrifugation. The cells were cultured in YES medium at 18 °C. Samples were then subjected to DAPI staining for determination of the percentage of cells entering mitosis.

To determine the role of CK2 in Mad2p localization, we used yeast strains in which Mad2p was tagged with the green fluorescent protein (GFP) [13] and monitored Mad2-GFP in cells lacking *ckb1*. The temperature was shifted to 18 °C at time 0 and the distribution of Mad2-GFP was determined. Mad2-GFP was observed in the nuclear periphery and chromatin domain in *nda3* and *nda3 ckb1* cells at 0 h (Fig. 2A and B). Whereas Mad2-GFP accumulated at kinetochores in *nda3* cells at 9 h, this increase was not observed in *nda3 ckb1* cells (Fig. 2A and B). These results suggest that *ckb1*⁺ is required for the localization of Mad2-GFP to unattached kinetochores.

Since Mad2p does not associate with unattached kinetochores in *ckb1* cells, we next tested whether ectopic expression of *mad2*⁺ could rescue the sensitivity of *ckb1* cells to TBZ (Fig. 2C). Ectopic

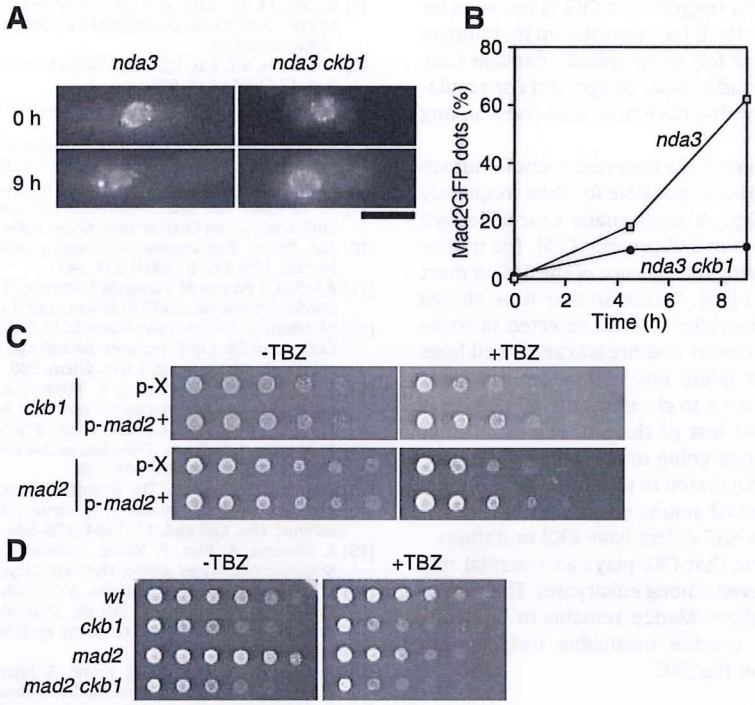


**Fig. 2.** CK2 is required for the localization of Mad2p at unattached kinetochores. (A, B) Cells (*nda3*, HM5170; *nda3 ckb1*, HM5741) were grown exponentially in EMM2 medium at 34 °C. (A) At time 0, the temperature was shifted to 18 °C. Mad2-GFP was visualized at the indicated times. Bar, 5 μm. (B) The percentage of cells with Mad2-GFP dots was determined. (C) Exponentially growing cells (*ckb1*, HM3584; *mad2*, HM1338) harboring pREP81-*mad2*$^+$ (p-*mad2*$^+$) or an empty vector (p-x) were spotted onto EMM plates without (−TBZ) or with 0.015 mg/ml TBZ (+TBZ). Plates were incubated at 32 °C for *ckb1* and at 30 °C for *mad2* for 3 days. (D) Exponentially growing cells (*wt*, HM4; *ckb1*, HM3584; *mad2*, HM1338; *mad2 ckb1*, HM5177) were spotted onto YES plates without (−TBZ) or with 0.015 mg/ml TBZ (+TBZ). Plates were incubated at 30 °C for 2 days.

expression of *mad2*$^+$ indeed restored viability to *ckb1*-deleted cells, as also observed for *mad2*-deleted cells after TBZ treatment. We thus concluded that *mad2*$^+$ functions downstream of *ckb1*$^+$.

To clarify the relative contributions of *ckb1*$^+$ and *mad2*$^+$ to the regulation of the SAC, we constructed a *mad2 ckb1* double mutant and monitored its viability after exposure to TBZ (Fig. 2D). The viability of *mad2 ckb1* cells was similar to that of the *ckb1* mutant, suggesting that *ckb1*$^+$ and *mad2*$^+$ act in the same pathway.

We next examined the effects of TBZ exposure on the abundance of Mad2p in CK2 mutants (Fig. 3A and B). The amount of Mad2p in *wt* cells did not vary after treatment of exponential cultures with TBZ at either 32 °C or 20 °C. In contrast, the amount of Mad2p in *ckb1* cells was low in the presence or absence of TBZ (Fig. 3A). The amount of Mad2p increased after heat shock treatment, whereas this increase was not observed in *orb5* cells (Fig. 3B). These results suggest that CK2 is partially required for the maintenance of Mad2p independent of the SAC activation. It is possible that in *ckb1* cells failure of the localization of Mad2-GFP to unattached kinetochores is due to the low protein level of Mad2p. However, it is unlikely since Mad2-GFP was detected in the nuclear periphery and chromatin domain in *ckb1* cells.

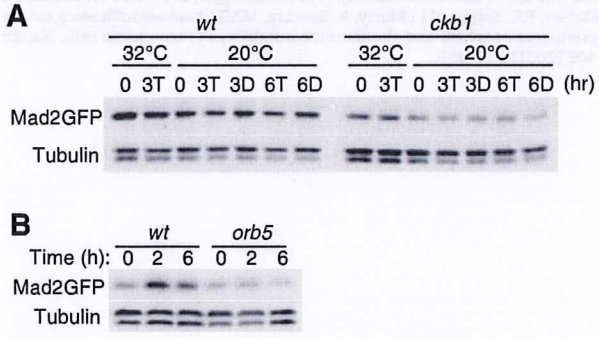


**Fig. 3.** The Mad2p level is low in CK2 mutants. (A) *wt* (HM5170) and *ckb1* (HM5172) cells were grown to mid-log phase in YES medium at 32 °C (32 °C, 0). TBZ (0.1 mg/ml) was added at time 0 and samples were collected after 3 h (32 °C, 3T). After the cells were grown at 32 °C, the temperature was shifted to 18 °C in YES medium without (D) or with TBZ (T). Samples were collected at the indicated times and subjected to immunoblot analysis using an anti-GFP antibody. (B) *wt* (HM5170) and *orb5* (HM5265) cells were grown to mid-log phase in YES medium at 24 °C. The temperature was shifted to 36 °C at time 0. Samples were analyzed as in (A).

We next tested whether protein levels and localization of Orb5p and Ckb1p change in response to activation of the SAC. The protein level did not vary with TBZ treatment (Supplementary figure 1). However, the levels of both proteins increased in *nda3* mutant cells compared with *wt* cells, but these levels did not change after the temperature shift. This result may reflect the fact that Orb5p and Ckb1p did not vary in response to SAC activation, but due to other defects in *nda3* cells. We found that Orb5p and Ckb1p were constitutively present in the nucleus with and without the activation of the SAC (Supplementary figure 2). In higher eukaryotes, CK2 is associated with centromeres and the mitotic spindle during mitosis [21]. It is likely that a sub-fraction of fission yeast CK2 is associated with the kinetochores, where it might regulate the localization of Mad2p when the SAC is activated.

We have shown that *ckb1* and *orb5* mutants exhibit the defining feature of a metaphase checkpoint defect — the failure to arrest in metaphase in the presence of spindle damage. In addition, these mutants show sensitivity to the microtubule-destabilizing drug TBZ. We have also found that Ckb1p is required for the localization of Mad2p to unattached kinetochores. In all of these respects, *ckb1* and *orb5* mutant phenotypes are qualitatively similar to those described for perturbations of the classical checkpoint components Mad1p and Mad2p. However, in *ckb1* and *orb5* mutants the protein

level of Mad2p is low. These facts suggest that CK2 is required for the SAC both directly and indirectly. It has been shown that human CK2 is involved in mitotic arrest following spindle damage [22]. We propose that CK2 represents additional components or regulators of the metaphase checkpoint that have been conserved among eukaryotes.

Loss of mitotic checkpoint control is a common event in human cancer cells, which is thought to be responsible for their frequently observed chromosome instability, although many cancer-derived samples do not contain mutations in SAC proteins [23]. The molecular nature of the defect underlying the absence of the SAC in most of these cell lines is not known [24]. Recent studies have shown that reduced levels of Mad2 expression can be detected in nasopharyngeal carcinoma, ovarian cancer and breast cancer cell lines and ovarian cancer [25,26]. Complete loss of Mad2p in various results in embryonic lethality owing to chromosome mis-segregation [27]. It is likely that partial loss of the SAC leads to tumor development in cells that are undergoing tumorigenesis. We have shown that the Mad2p level is decreased in CK2 mutants in fission yeast. Since CK2 is highly conserved among eukaryotes, it is possible that tumor cells harboring a SAC defect have CK2 mutations.

In conclusion, we have shown that CK2 plays an essential role on the SAC that has been conserved among eukaryotes. The molecular mechanism how CK2 regulates Mad2p remains to be determined. Future studies should provide invaluable insights into understanding the role of CK2 in the SAC.

## Acknowledgments

We thank P. Nurse and T. Toda for yeast strains and K. Okazaki for plasmids and helpful discussion. This work was supported in part by a grant-in-aid for Scientific Research from the Ministry of Education, Culture, Sports, Science, and Technology of Japan (to H.M. and Y.M-T.).

## Appendix A. Supplementary data

Supplementary data associated with this article can be found, in the online version, at doi:10.1016/j.bbrc.2009.08.030.

## References

[1] D.W. Cleveland, Y. Mao, K.F. Sullivan, Centromeres and kinetochores: from epigenetics to mitotic checkpoint signaling, Cell 112 (2003) 407–421.
[2] S. Hauf, Y. Watanabe, Kinetochore orientation in mitosis and meiosis, Cell 119 (2004) 317–327.
[3] H. Murakami, P. Nurse, DNA replication and damage checkpoints and meiotic cell cycle controls in the fission and budding yeasts, Biochem. J. 349 (2000) 1–12.
[4] A. Musacchio, E.D. Salmon, The spindle-assembly checkpoint in space and time, Nat. Rev. Mol. Cell Biol. 8 (2007) 379–393.
[5] L.J. Vos, J.K. Famulski, G.K. Chan, How to build a centromere: from centromeric and pericentromeric chromatin to kinetochore assembly, Biochem. Cell Biol. 84 (2006) 619–639.
[6] G.K. Chan, S.T. Liu, T.J. Yen, Kinetochore structure and function, Trends Cell Biol. 15 (2005) 589–598.
[7] R. Karess, Rod-Zw10-Zwilch: a key player in the spindle checkpoint, Trends Cell Biol. 15 (2005) 386–392.
[8] E. Montembault, S. Dutertre, C. Prigent, R. Giet, PRP4 is a spindle assembly checkpoint protein required for MPS1, MAD1, and MAD2 localization to the kinetochores, J. Cell Biol. 179 (2007) 601–609.
[9] M. Yanagida, Cell cycle mechanisms of sister chromatid separation; Roles of Cut1/separin and Cut2/securin, Genes Cells 5 (2000) 1–8.
[10] J.M. Peters, The anaphase-promoting complex: proteolysis in mitosis and beyond, Mol. Cell 9 (2002) 931–943.
[11] A.E. Ikui, K. Furuya, M. Yanagida, T. Matsumoto, Control of localization of a spindle checkpoint protein, Mad2, in fission yeast, J. Cell Sci. 115 (2002) 1603–1610.
[12] M. Shimada, C. Namikawa-Yamada, M. Nakanishi, H. Murakami, Regulation of Cdc2p and Cdc13p is required for cell cycle arrest induced by defective RNA splicing in fission yeast, J. Biol. Chem. 280 (2005) 32640–32648.
[13] I. Sugimoto, H. Murakami, Y. Tonami, A. Moriyama, M. Nakanishi, DNA replication checkpoint control mediated by the spindle checkpoint protein Mad2p in fission yeast, J. Biol. Chem. 279 (2004) 47372–47378.
[14] F. Meggio, L.A. Pinna, One-thousand-and-one substrates of protein kinase CK2?, FASEB J 17 (2003) 349–368.
[15] I. Roussou, G. Draetta, The *Schizosaccharomyces pombe* casein kinase II alpha and beta subunits: evolutionary conservation and positive role of the beta subunit, Mol. Cell Biol. 14 (1994) 576–586.
[16] S. Moreno, A. Klar, P. Nurse, Molecular genetic analysis of fission yeast *Schizosaccharomyces pombe*, Methods Enzymol. 194 (1991) 795–823.
[17] J. Bahler, J.Q. Wu, M.S. Longtine, N.G. Shah, A. McKenzie 3rd, A.B. Steever, A. Wach, P. Philippsen, J.R. Pringle, Heterologous modules for efficient and versatile PCR-based gene targeting in *Schizosaccharomyces pombe*, Yeast 14 (1998) 943–951.
[18] K. Okazaki, N. Okazaki, K. Kume, S. Jinno, K. Tanaka, H. Okayama, High-frequency transformation method and library transducing vectors for cloning mammalian cDNAs by trans-complementation of *Schizosaccharomyces pombe*, Nucleic Acids Res. 18 (1990) 6485–6489.
[19] H. Murakami, P. Nurse, Meiotic DNA replication checkpoint control in fission yeast, Genes Dev. 13 (1999) 2581–2593.
[20] T. Toda, K. Umesono, A. Hirata, M. Yanagida, Cold-sensitive nuclear division arrest mutants of the fission yeast *Schizosaccharomyces pombe*, J. Mol. Biol. 168 (1983) 251–270.
[21] W. Krek, G. Maridor, E.A. Nigg, Casein kinase II is a predominantly nuclear enzyme, J. Cell Biol. 116 (1992) 43–55.
[22] M. Sayed, S. Pelech, C. Wong, A. Marotta, B. Salh, Protein kinase CK2 is involved in G2 arrest and apoptosis following spindle damage in epithelial cells, Oncogene 20 (2001) 6994–7005.
[23] C.S. Lopes, C.E. Sunkel, The spindle checkpoint: from normal cell division to tumorigenesis, Arch. Med. Res. 34 (2003) 155–165.
[24] T. Takahashi, N. Haruki, S. Nomoto, A. Masuda, S. Saji, H. Osada, T. Takahashi, Identification of frequent impairment of the mitotic checkpoint and molecular analysis of the mitotic checkpoint genes, hsMAD2 and p55CDC, in human lung cancers, Oncogene 18 (1999) 4295–4300.
[25] X. Wang, D.Y. Jin, Y.C. Wong, A.L. Cheung, A.C. Chun, A.K. Lo, Y. Liu, S.W. Tsao, Correlation of defective mitotic checkpoint with aberrantly reduced expression of MAD2 protein in nasopharyngeal carcinoma cells, Carcinogenesis 21 (2000) 2293–2297.
[26] M.J. Percy, K.A. Myrie, C.K. Neeley, J.N. Azim, S.P. Ethier, E.M. Petty, Expression and mutational analyses of the human MAD2L1 gene in breast cancer cells, Genes Chromosomes Cancer 29 (2000) 356–362.
[27] L.S. Michel, V. Liberal, A. Chatterjee, R. Kirchwegger, B. Pasche, W. Gerald, M. Dobles, P.K. Sorger, V.V. Murty, R. Benezra, MAD2 haplo-insufficiency causes premature anaphase and chromosome instability in mammalian cells, Nature 409 (2001) 355–359.

# Cyclin A–Cdk1 regulates the origin firing program in mammalian cells

Yuko Katsuno[a], Ayumi Suzuki[a], Kazuto Sugimura[b], Katsuzumi Okumura[b], Doaa H. Zineldeen[a], Midori Shimada[a], Hiroyuki Niida[a], Takeshi Mizuno[c], Fumio Hanaoka[c,d], and Makoto Nakanishi[a,1]

[a]Department of Cell Biology, Graduate School of Medical Sciences, Nagoya City University, 1 Kawasumi, Mizuho-cho, Mizuho-ku, Nagoya 467-8601, Japan; [b]Laboratory of Molecular and Cellular Biology, Graduate School of Bioresources, Mie University, 1577 Kurimamachiya-cho, Tsu, Mie 514-8507, Japan; [c]Cellular Physiology Laboratory, RIKEN Discovery Research Institute, and Solution Oriented Research for Science and Technology, Science and Technology Corporation, Wako, Saitama 351-0198, Japan; and [d]Faculty of Science, Gakushuin University, Toshima, Tokyo 171-8588, Japan

Edited by Tak Wah Mak, University of Toronto, Toronto, Canada, and approved January 12, 2009 (received for review September 18, 2008)

**Somatic mammalian cells possess well-established S-phase programs with specific regions of the genome replicated at precise times. The ATR–Chk1 pathway plays a central role in these programs, but the mechanism for how Chk1 regulates origin firing remains unknown. We demonstrate here the essential role of cyclin A2–Cdk1 in the regulation of late origin firing. Activity of cyclin A2–Cdk1 was hardly detected at the onset of S phase, but it was obvious at middle to late S phase under unperturbed condition. Chk1 depletion resulted in increased expression of Cdc25A, subsequent hyperactivation of cyclin A2–Cdk1, and abnormal replication at early S phase. Hence, the ectopic expression of cyclin A2–Cdk1AF (constitutively active mutant) fusion constructs resulted in abnormal origin firing, causing the premature appearance of DNA replication at late origins at early S phase. Intriguingly, inactivation of Cdk1 in temperature-sensitive Cdk1 mutant cell lines (FT210) resulted in a prolonged S phase and inefficient activation of late origin firing even at late S phase. Our results thus suggest that cyclin A2–Cdk1 is a key regulator of S-phase programs.**

Chk1 | DNA replication | molecular combing | ATR protein | checkpoint

Duplication of the eukaryotic genome is regulated by multiple elements including initiation of DNA replication, rate of fork progression, stability of replication forks, and the origin firing program (1). Replication origins are fired in small groups that are activated together within individual replication factories and thus can be visualized as foci (2). Replication origins in a single replication factory are actually comprised of several candidate origins, most of which are not normally used through the mechanism by which firing of 1 origin inhibits activation of any other Mcm2–7 complexes within that factory (3). Thus, S-phase programs appear to be regulated by 2 distinct levels of origin firing; one is the sequential activation of replicon clusters characterized as visible replication foci, and the other is the selection of 1 Mcm2–7 complex around the ORC within a single replication factory.

The DNA replication checkpoint system was reported to be involved in the origin firing program in vertebrate cells (4). In analysis using *Xenopus* egg extract, ATR/Chk1 was shown to regulate the sequential activation of early and late replication origins (5). Chk1 also regulates the density of active replication origins during S phase of avian cells (6). Therefore, ATR/Chk1 may be involved in the regulation of sequential activation of replicon clusters and selection of origins within a single replication factory. Chk1 has been shown to regulate the physiological turnover of Cdc25A and its phosphatase activity, which in turn regulates several cyclin–Cdk activities (7) that are prerequisite for origin firing throughout S phase.

In budding yeast, Clb5-dependent Cdk activity is indispensable for activation of late replication origins (8), suggesting the existence of a specific transfactors for late origin activation in other eukaryotes. In fission yeast, however, clear late origins have not been characterized (9) and replication origins fire stochastically (10, 11). As for mammals, although almost half of origins are activated equally throughout S-phase progression (12), stable subunits of chromosomes equivalent to replication foci maintain their replication timing from S phase to S phase (13).

In this article, we demonstrate that Chk1 depletion resulted in an aberrant origin firing and a hyperactivation of cyclin A2–Cdk1 at early S phase. Ectopic expression of cyclin A2–Cdk1AF induced late origin firing at early S phase, and a loss of Cdk1 activity compromised activation of late origins at late S phase. Our results thus suggested that cyclin A2–Cdk1 might function as a transregulator of late origin firing in mammals.

## Results

**Chk1 Depletion Results in an Aberrant Origin Firing and a Hyperactivation of Cyclin A2–Cdk1 at Early S Phase.** $Chk1^{lox/-}$ mouse embryonic fibroblasts (MEFs) were infected with adenoviruses expressing either LacZ or Cre and synchronized into $G_0$ phase by serum starvation (14). $Chk1^{lox/-}$ and $Chk1^{del/-}$ MEFs were then stimulated by 15% serum and double-labeled with iododeoxyuridine (IdU) and chlorodeoxyuridine (CIdU) at the indicated times, and their spatiotemporal patterns of replication sites were examined. The mammalian S phase is structured so that the sequential activation of replicon clusters occurs at spatially adjacent sites (15). This spatial relationship is maintained in $Chk1^{lox/-}$ MEFs (Fig. 1*A*), where 86.6 ± 4.4 of foci showed colocalization visualized as yellow color. In contrast, colocalization was detected only at 53.9 ± 4.8 of foci in $Chk1^{del/-}$ MEFs (Fig. 1*B*), indicating that Chk1 depletion in mammals resulted in the aberrant origin firing as observed in avian cells (6). Molecular combing of single DNA molecules was performed to visualize individual origin activation, measure the fork elongation, and define replication structures (Fig. 1*C* and Fig. S1). In asynchronized $Chk1^{lox/-}$ MEFs infected with control LacZ adenoviruses interorigin spacing (90.4 kb on average) was similar to that in mock-infected cells. Chk1 depletion resulted in a clear reduction in origin spacing (34.8 kb on average)(Fig. 1*C Top*). Spatiotemporal pattern of replication sites could also be affected by fork elongation. Chk1 depletion reduced the rate of fork elongation throughout the labeling period (Fig. 1*C Middle*).

Double-labeling protocol also defines 5 classes of replication structure as described (6). Chk1 depletion resulted in a significant reduction in a proportion of consecutively elongating forks (class 1) and an increase in number of new firing initiation during the first (class 2) and second (class 4) labeling period (Fig. 1*C Bottom*). A dramatic increase in the frequency of closely-spaced active origins

Author contributions: M.N. designed research; Y.K., A.S., K.S., K.O., D.H.Z., M.S., and H.N. performed research; T.M. and F.H. contributed new reagents/analytic tools; Y.K., K.S., and M.N. analyzed data; and Y.K. and M.N. wrote the paper.

The authors declare no conflict of interest.

This article is a PNAS Direct Submission.

[1]To whom correspondence should be addressed. E-mail: mkt-naka@med.nagoya-cu.ac.jp.

This article contains supporting information online at www.pnas.org/cgi/content/full/0809350106/DCSupplemental.



www.pnas.org/cgi/doi/10.1073/pnas.0809350106

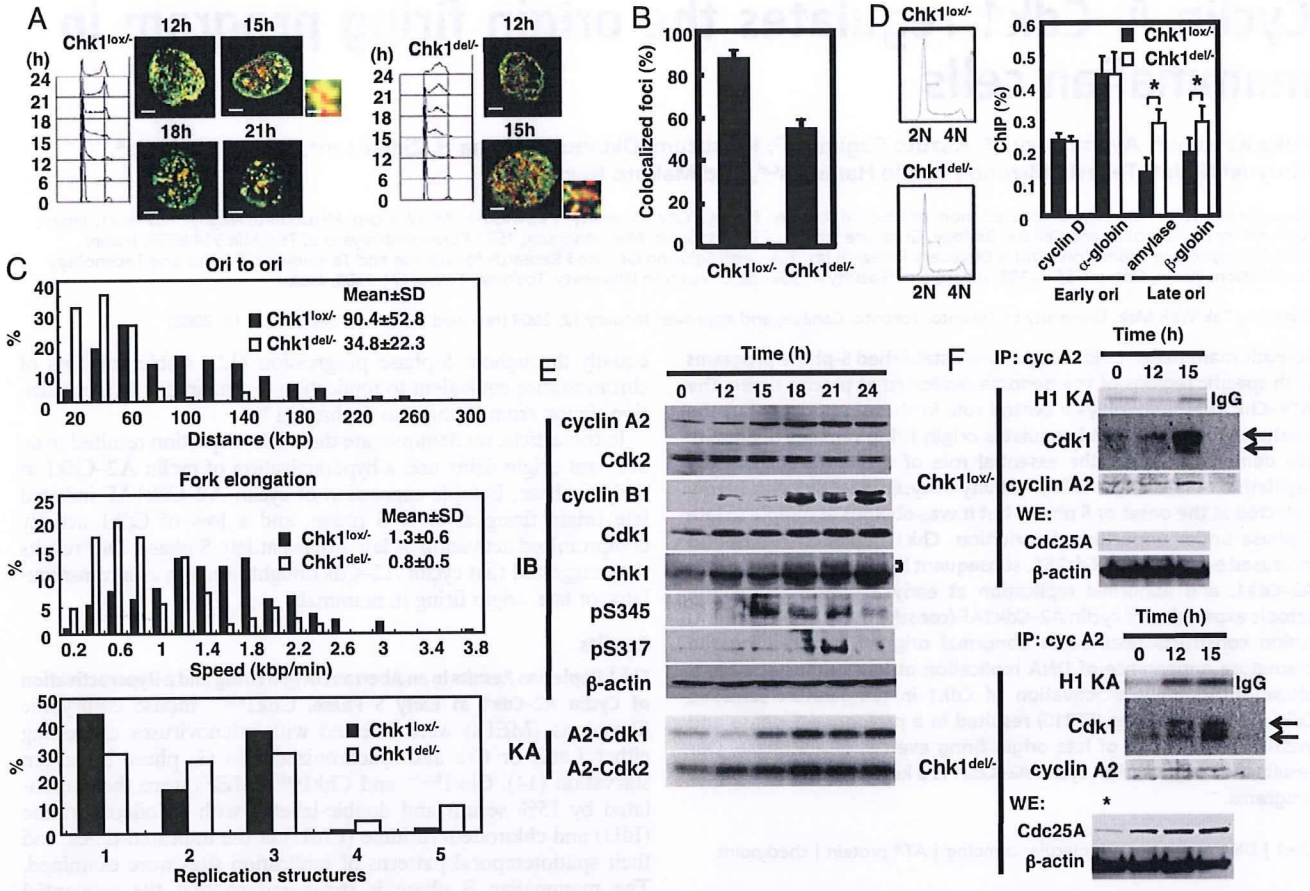


**Fig. 1.** Chk1 depletion results in an aberrant S-phase program and an activation of cyclin A2–Cdk1 at early S phase. (*A*) Chk1$^{lox/-}$ and Chk1$^{del/-}$ MEFs were synchronized at quiescence by serum starvation and then released by the addition of 15% serum. Cells were harvested at the indicated times, and their cell cycle distributions were analyzed by FACS. Replication sites were pulse-labeled for 15 min with 100 $\mu$M IdU and then for 15 min with 100 $\mu$M CldU, and analyzed with a Zeiss LSM5 confocal fluorescence microscope. Typical patterns of replication sites at the indicated times are presented. High-power details are from the boxed areas shown. (Scale bars: 5 and 0.5 $\mu$m in detail.) (*B*) Colocalization of IdU and CldU foci in Chk1$^{lox/-}$ and Chk1$^{del/-}$ MEFs. Relative colocalization of IdU and CldU foci was determined as a percentage of total foci in both cells ($n > 30$). Data are means ± SD of at least 3 independent experiments. (*C*) Asynchronized Chk1$^{lox/-}$ MEFs were infected with the indicated adenoviruses and double-labeled with IdU and CldU before harvesting at 28 h after infection. Replication structures were visualized by means of dynamic molecular combing. Adjacent origins in replicon clusters (Ori to ori), fork elongation, and replication structure defined by ref. 6 were determined ($n > 100$). Frequency histograms show the distribution of separation in distance (kbp), speed (kbp/min), and replication structure (1, elongating fork; 2, fork growing from 1 ori; 3, terminal fusions; 4, isolated; 5, interspersed). (*D*) Asynchronized Chk1$^{lox/-}$ MEFs were infected with adenoviruses expressing either LacZ or Cre. Cells were labeled with BrdU for 1 h before harvesting at 28 h after infection, and the cell cycle profiles were then analyzed by FACS. Early S-phase fraction indicated by bars was sorted, and nascent DNA was enriched by immunoprecipitation using $\alpha$-BrdU. The indicated genes were amplified by quantitative PCR, and the results are presented as a percentage of mtDNA. Data are means ± SD of at least 3 independent experiments. Statistical significance was assessed by Student's *t* test (*, $P < 0.01$). (*E*) Synchronized Chk1$^{lox/-}$ MEFs as in *A* were harvested at the indicated times, and the lysates were subjected to immunoblotting by using the indicated antibodies or to an in vitro kinase assay (KA) for cyclin A2–Cdk1 and cyclin A2–Cdk2 with HH1 (2 $\mu$g) as a substrate. (*F*) Synchronized Chk1$^{lox/-}$ and Chk1$^{del/-}$ MEFs as in *A* were harvested at the indicated times, and the lysates were immunoprecipitated by using $\alpha$-cyclin A2 antibodies after 3 times preabsorbance with $\alpha$-Cdk2. The resultant immunoprecipitates (IP: cyclin A2) or whole-cell extracts (WE) were subjected to immunoblotting or in vitro kinase assay as in *E*. Arrows indicate the fast (active) or slow (inactive) migrated bands of Cdk1. An asterisk represents cell lysates from Chk1$^{lox/-}$ MEFs at 15 h.

(class 5) was observed. These observations suggest that loss of Chk1 frequently stalls and collapses active forks.

We next examined whether Chk1 regulates global sites of DNA synthesis by quantitative ChIP using FACS-based cell sorting (16). To avoid unexpected effects from gross changes in cell cycle profile on this analysis, we analyzed Chk1$^{del/-}$ MEFs 28 h after adenoviral infection, the time at which Chk1 was completely depleted, but the cell cycle profile was almost the same as that of Chk1$^{lox/-}$ cells (Fig. 1*D*). Cells from the first third of S phase were collected (Fig. 1*D Left*). Nascent (BrdU-containing) DNA was enriched by immunoprecipitation using $\alpha$-BrdU antibodies and amplified by quantitative PCR with specific primers for cyclin D and $\alpha$-globin for early-replicating DNA and primers for amylase and $\beta$-globin for late-replicating DNA. We also monitored amplification of mtDNA as a control, which replicates throughout the cell cycle and is equally represented in nascent DNA preparations (16, 17). The relative amounts of early replication (cyclin D and $\alpha$-globin) in Chk1$^{del/-}$ MEFs were almost the same as those in Chk1$^{lox/-}$ cells, whereas those of late replication (amylase and $\beta$-globin) in Chk1$^{del/-}$ MEFs were significantly higher than those in Chk1$^{lox/-}$ cells (Fig. 1*D Right*). Given that 1 cell possesses ≈1,000 copies of mitochondrial genome, but they replicate throughout the cell cycle, relative amplification of nascent DNA (≈0.3) for early and late origins appeared consistent.

Chk1 is phosphorylated during unperturbed S phase (18, 19), which regulates the activity and stability of Cdc25 phosphatases, leading to the inactivation of Cdks through increased phosphorylation of their Y15 residues (20). Thus, we speculated that Chk1

regulates origin firing program through affecting certain cyclin–Cdks activities. The band corresponding to Chk1 was shifted upward at 15 h and thereafter. This band shift was reversed by phosphatase treatment, indicating that the modification was caused by phosphorylation. Chk1 phosphorylation was also confirmed by using phospho-specific antibodies to Chk1 at Ser-317 and Ser-345 (Fig. 1*E*).

Cyclin A2–Cdk1 activity was first detected at 15 h (middle S phase) and increases thereafter. Cyclin A2–Cdk2 was detected at 6 h (early S phase) and reached maximum at 18 h (Fig. 1*E* and Fig. S2*A*). These results are consistent with the recent report that cyclin A2 starts to form a complex with Cdk1 at mid-S phase (21). Cyclin A2–Cdk1 activity was detected earlier and enhanced in $Chk1^{del/-}$ MEFs when compared with $Chk1^{lox/-}$ MEFs (Fig. 1*F*), where immunodepletion of Cdk2 was equally achieved in both cyclin A2 immunoprecipitates (Fig. S2*B*). Cyclin A2–Cdk2 activity was not apparently affected by Chk1 depletion (Fig. S2*A*). Intriguingly, the amount of Cdc25A was highly elevated in $Chk1^{del/-}$ MEFs. Consistent with this increase in amount of Cdc25A, fast mobility band (active; Y15 dephosphorylation) and slow band (inactive; Y15 phosphorylation) of Cdk1 protein were dominant in those from $Chk1^{del/-}$ MEFs and $Chk1^{lox/-}$ MEFs, respectively (Fig. 1*F*). Specificity of cyclin A2–Cdk1 activity was confirmed by Cdk1 knockdown experiment, where cyclin A2–Cdk1 activities in both MEFs were significantly reduced after Cdk1 depletion (Fig. S3). To further confirm the functional interaction between Chk1 and cyclin A2–Cdk1, $Chk1^{lox/-}$ MEFs were treated with UV light, which phosphorylated Chk1 in an ATR-dependent manner. Chk1 phosphorylation was correlated with the reduction of Cdc25A, the appearance of slow mobility band of Cdk1 protein, and inhibition of cyclin A2–Cdk1 activity (Fig. S4). Taken together, cyclin A2–Cdk1 is likely to be a target of Chk1 through regulation of Cdc25A.

**Aberrant Origin Firing in Cells Expressing Cyclin A2–Cdk1AF Fusion Protein.** To examine the role of each cyclin–Cdk complex in the origin firing program, we generated a cyclin A2–Cdk1 fusion construct. Because cyclin–Cdk activities are regulated mainly by the phosphorylation of Y15, we generated a constitutively active mutant (CdkAF) in which residues at inhibitory phosphorylation sites were replaced with alanine and phenylalanine and therefore the mutant was not affected by the Chk1–Cdc25 pathway. Recombinant cyclin A2–Cdk2AF, cyclin A2–Cdk1AF, and cyclin B1–Cdk1AF complexes and the fusion proteins were examined for their enzymatic kinetics by using histone H1 (HH1) and lamin B as substrates. Dose-dependent increases in activities of both cyclin–Cdks complex and their fusion proteins were observed (Fig. 2*A*). The kinetic values of these complexes were the same as those of the fusion proteins (Table S1).

Expression of cyclin B1–Cdk1AF, but not cyclin A2–Cdk2AF or cyclin A2–Cdk1AF, induced γH2AX foci in HeLa cells (Fig. 2*B*). Amounts of cyclin B1–Cdk1AF, cyclin A2–Cdk1, and cyclin A2–Cdk2 fusion proteins expressed at 24 h after infection were almost equal to endogenous Cdk1 and Cdk2 proteins, respectively (Fig. 2*C* and Fig. S5). Again, γH2AX was not detected by immunoblotting in cells expressing cyclin A2–Cdk1 or cyclin A2–Cdk2 fusion protein.

Expression of cyclin A2–Cdk1AF and cyclin A2–Cdk2AF fusion protein at the endogenous level did not appear to affect the gross progression of S phase (Fig. 3*A*) although they arrested the cell cycle at M phase because of their inability to be degraded by APC-C at mitosis and thus mitotic exit was inhibited. The expression of cyclin A2–Cdk1AF fusion protein caused the appearance of late replication sites during early S phase when cells were double-labeled with IdU and CIdU (Fig. 3*B*). Dynamic molecular combing revealed that expression of cyclin A2–Cdk1AF fusion protein reduced origin spacing (75.0 kb on average), whereas that of cyclin A2–Cdk2AF

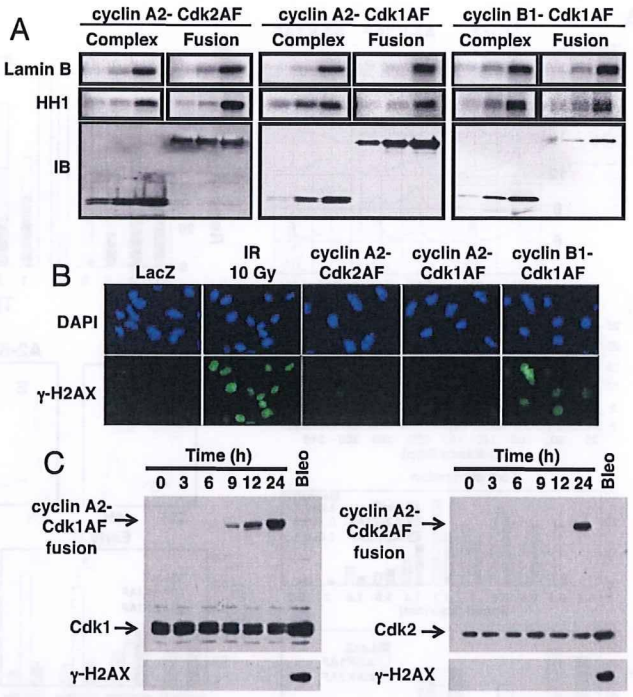


**Fig. 2.** Enzymatic kinetics of cyclin–Cdk fusion proteins. (*A*) Baculoviruses expressing cyclin A2 together with those expressing Cdk2 or Cdk1 (Complex) or those expressing cyclin A2–Cdk2, cyclin A2–Cdk1, or cyclin B1–Cdk1 fusion protein (Fusion) were used to infect insect cells. Their complexes or fusion proteins were purified and subjected to an in vitro kinase assay using lamin B (2 μg) or HH1 (2 μg) as a substrate or subjected to immunoblotting by using Cdk2 or Cdk1 antibodies (IB). (*B*) HeLa cells were infected with adenoviruses expressing the indicated proteins 24 h before fixing and immunostained with α-γH2AX antibodies. Their nuclei were counterstained with DAPI. As a positive control, cells infected with adenoviruses expressing LacZ were treated with IR (10 Gy). (Magnifications: 100×.) (*C*) HeLa cells were infected with adenoviruses expressing either cyclin A2-Cdk1AF or cyclin A2-Cdk2AF fusion proteins. Cells were harvested at the indicated times, and the lysates were subjected to immunoblotting using α-Cdk1 (*Upper Left*), α-Cdk2 (*Upper Right*), or α-γH2AX antibodies (*Lower*). As a control, HeLa cells were treated with bleomycin for 24 h (20 μg/mL).

did not (113.0 kb on average)(Fig. 3*C Top* and Fig. S6). Unlike Chk1 depletion, expression of cyclin A2–Cdk2AF did not cause significant changes in the proportion of abnormal replication structures (Fig. 3*C Bottom*). Taken together, these results suggested that cyclin A2–Cdk1 had a specific role in the origin firing program.

ChIP analysis revealed that considerable enrichment of early- and late-replicating DNA was specifically observed in the early and late S-phase fractions of control LacZ cells, respectively (Fig. 3*D*). Ectopic expression of cyclin A2–Cdk1AF resulted in the dramatic increase in replication of late origins in early S-phase fractions, but that of cyclin A2–Cdk2AF did not apparently affect it.

**Cdk1 Is Required for Proper Timing of Origin Firing.** FT210 cells possess a temperature-sensitive Cdk1 gene product (22). FACS analysis revealed a 2-h-longer S phase in FT210 cells compared with the parental FM3A cells (Fig. 4*A*). S-phase progression of FT210 cells at a permissive temperature was almost the same as that of FM3A cells. The progression of the spatiotemporal pattern of DNA replication sites in FM3A at the nonpermissive temperature was almost the same as in HeLa cells or MEFs. In contrast, the specific pattern of DNA replication sites observed in late S phase showing a few large internal foci was hardly detected in FT210 cells even at late S phase at nonpermissive temperature (Fig. 4*A*). Loss of Cdk1

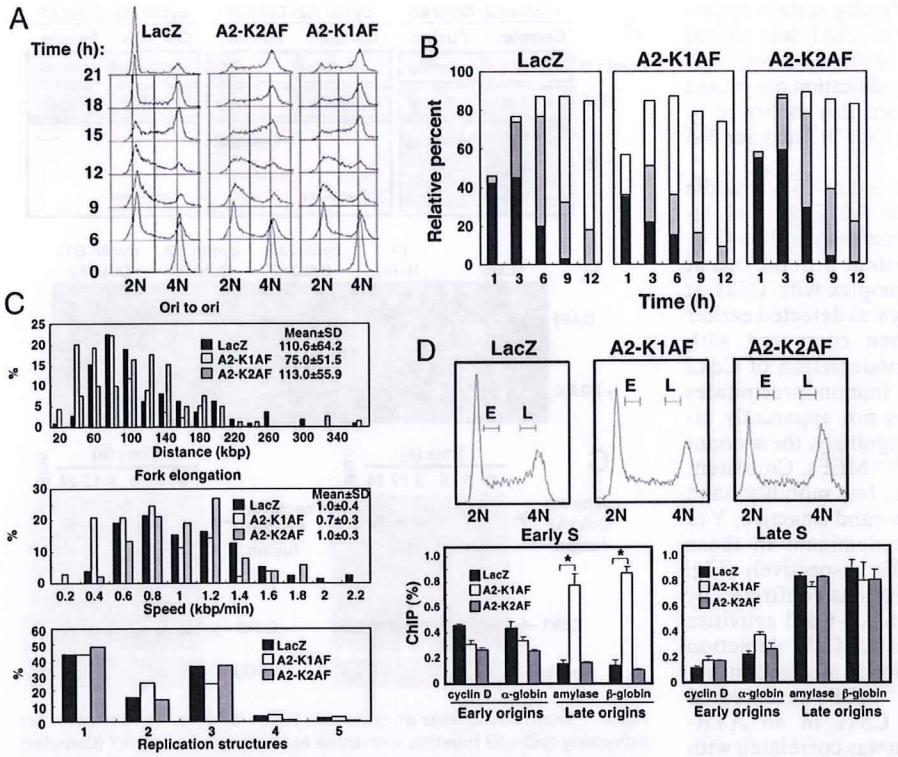


**Fig. 3.** Ectopic expression of cyclin A2-Cdk1AF, but not cyclin A2–Cdk2AF resulted in an aberrant temporal regulation of origin firing. (*A*) HeLa cells were synchronized by thymidine (2 mM, 24 h)/release period (6 h)/nocodazole (0.1 μg/mL, 12 h) and infected with adenoviruses expressing either cyclin A2–Cdk2AF, cyclin A2–Cdk1AF, or LacZ (control) 12 h before nocodazole washout (time 0). Cells were harvested at the indicated times, and their cell cycle profiles were analyzed by FACS. (*B*) HeLa cells were infected with the indicated adenoviruses 24 h before mimosine (0.6 mM, 16 h) washout (time 0). Replication sites were pulse-labeled for 15 min with IdU (100 μM) and then for 15 min with CldU (100 μM) before harvesting at the indicated times. The number of replication sites of each pattern was counted, and the relative percentage of the total number of cells ($n > 300$) is indicated. Black bars represent the early pattern, gray bars represent the middle pattern, and white bars represent the late pattern. Data are means of at least 3 independent experiments. (*C*) Asynchronous HeLa cells were infected with the indicated adenoviruses. Cells were harvested 24 h after infection and subjected to molecular combing. Adjacent origins in replicon clusters (Ori to ori), fork elongation, and replication structure were determined ($n > 100$) as in Fig. 1*C*. (*D*) Asynchronous HeLa cells infected with the indicated adenoviruses were pulse-labeled with BrdU before harvesting cells 24 h after infection. S-phase cells were then sorted into early (E) or late (L) fractions (*Upper*). The sorted cells were collected, and replication firing at the indicated origins was analyzed by ChIP analysis (*Lower*) as in Fig. 1*D*. Data are means ± SD of at least 3 independent experiments. Statistical significance was assessed by Student's *t* test (*, $P < 0.01$).

resulted in a significant increase in origin spacing (104.7 kb on average) when compared with control cells (78.6 kb on average) (Fig. 4*B Top* and Fig. S6). Loss of Cdk1 did not cause changes in the proportion of replication structures, further supporting the notion that Cdk1 is not involved in the stabilization of replication forks.

ChIP analysis revealed that replication patterns of early S-phase fractions in both cells were very similar, whereas replication of late origins in late S-phase fraction from FT210 cells was specifically impaired (Fig. 5*A Right*). Cdk2 activity during S phase in FT210 cells appeared the same as that in FM3A cells (Fig. S7). Collectively, these results suggested that Cdk1 activity is involved in the proper timing of late origin firing.

Finally, we attempted to determine the molecular basis by which cyclin A2–Cdk1 regulates origin firing program. In *Xenopus* and yeast systems, it was reported that cyclins, Cdk1 specifically, interact with the origin recognition complexes (ORCs) (23, 24). To examine whether the specific interaction of Cdk1 to ORCs is conserved among mammals, we performed ChIP analysis with α-Cdk1 and α-Cdk2 antibodies. Both Cdk1 and Cdk2 were detected at genes replicating early, whereas Cdk1 was specifically detected at genes replicating late (Fig. 5*B*). Relative binding of Cdk1 and Cdk2 appeared somewhat low, presumably because of an asynchronous cell cycle. These results suggested that the specific binding of Cdk1 to late origins may also be involved in the regulation of origin firing programs.

## Discussion

Conditional Chk1 knockout MEFs revealed that Chk1 plays an important role in the regulation of origin firing at 2 distinct levels in mammals, namely activation of origins within a single replication factory and activation of replicon clusters (Fig. 1 *A–D*). Consistent with our observations, it was very recently proposed that Chk1 suppresses initiation in both inactive, later-firing clusters and active clusters, and the former is more strongly repressed (25). We then successfully showed that expression of cyclinA2–Cdk1AF fusion proteins activated origin firing at both levels as Chk1 depletion did (Fig. 3 *B–D*). The expression patterns of Cdk1 and cyclins during S phase and the enhancement of their activities in response to Chk1 depletion are also consistent with our conclusions (Fig. 1 *E* and *F*). The most striking evidence for the involvement of Cdk1 in DNA replication is the fact that inactivation of Cdk1 in mammalian cells resulted in a prolonged S phase accompanied by ineffective firing of late replicon clusters and reduced the density of active origins (Figs. 4 and 5*A*). Although our present results clearly demonstrate that cyclin A2–Cdk1 is involved in the regulation of late origin firing, functioning downstream of Chk1, we cannot rule out the possibility that cyclin A2–Cdk2 has a redundant function. Hochegger *et al.* (26) reported that Cdk1 activity was essential for DNA replication initiation when Cdk2 was depleted in chicken DT40 cells. When Cdk2 was present, Cdk1 inhibition did not delay S phase or block centrosome duplication. In this regard, DNA replication in DT40 cells appears complete within a shorter period (8 h) when compared with mammalian cells (10 h at 37 °C). Therefore, it is possible that DT40 cells possess a strong Cdk2 activity, presumably because of a loss of functional p53 that reduces the level of p21 Cdk inhibitor, and the high Cdk2 activity may compensate for the loss of Cdk1 activity in the context of S-phase control. In agreement with this notion, both Cdk1 and Cdk2 were recently reported to be involved in the control of DNA replication and replication origin firing under unperturbed S phase in the *Xenopus* system (27). It was also suggested that Cdk1 and Cdk2 must have different activities toward the genuine substrates involved in DNA replication although one kinase alone is minimally sufficient to promote substantial DNA replication.

Neither cyclin A2–Cdk1 nor cyclin A2–Cdk2 appeared to be involved in the stabilization of replication forks during S phase